Raman-probes to Monitor the Metabolite Detection and Assessment of Nutrient Fate of the *Yarrowia lipolytica* Cells Grown in Deuterated Glucose

A Thesis
Presented in Partial Fulfillment of the Requirements for the

Degree of Master of Science
with a
Major in Environmental Sciences
in the
College of Graduate Studies
University of Idaho
by

Gurkeerat Kukal

Major Professor: Armando G. McDonald, Ph.D.

Committee Members: Andreas Vasdekis, Ph.D.; Lili Cai, Ph.D.

Department Administrator: Lee Verling, Ph.D.

May 2021

Authorization to Submit Thesis

This thesis of Gurkeerat Kukal submitted for the degree of Master of Science with a Major in Environmental Sciences and titled "Raman-probes to Monitor the Metabolite Detection and Assessment of Nutrient Fate of the *Yarrowia lipolytica* Cells Grown in Deuterated Glucose," has been reviewed in final form. Permission, as indicated by the signatures and dates below, is now granted to submit final copies to the College of Graduate Studies for approval.

Major Professor: _____ Date: _____

Armando G. McDonald, Ph.D.

Committee Members: _____ Date: _____

Andreas Vasdekis, Ph.D.

_____ Date: _____

Lili Cai, Ph.D.

Department Administrator: _____ Date: _____

Lee Verling, Ph.D.

Abstract

Yarrowia lipolytica has been identified as a highly productive organism for the biosynthesis of triacyl glycerides (lipids) which can be converted into biofuels. To monitor lipid droplet production in the cell, Raman-based methods show promise when using deuterated probes for detection in the Raman-silent region (1800–2600 cm^{-1}). The study involves the use of deuterated labeled glucose as Raman tag-based assessment of the *Y. lipolytica* MTYL038 strain cells for the multifold monitoring of glucose uptake, consumption, and lipid biosynthesis. The cells were grown in yeast extract peptone dextrose followed by growth in three different synthetic media with no nitrogen (N) with glucose in H_2O, glucose-D_7 in H_2O and glucose D_7 in D_2O. The cells were grown under optimum conditions (96 h) in synthetic media to an optical density >2.5. The changes in biomass and lipid yields were observed. Fourier-transform infrared and Raman spectroscopies showed the incorporation of deuterium with the presence of a C-D bands in the Raman silent region (1800-2600 cm^{-1}) for both the glucose-d_7 and glucose-D_7 in D_2O grown cells. The fatty acid profiles for the extracted cells grown in the three media showed significant differences in lipid profiles. The cells grown on both glucose-D_7 media showed deuterium incorporation in the fatty acids as determined by mass spectrometry. This approach of labeling fatty acids can be used to monitor lipogenesis by Raman microscopy.

Acknowledgements

This journey would not have been possible without the support of my advisor, Dr. Armando McDonald. Throughout the two Academic years that I have spent at the University of Idaho, Dr. McDonald has helped me settle down in Renewable Materials Lab and has provided his valuable knowledge at every step of my research work. I feel honored to have had the chance to work with him during my Masters. I would also like to extend my sincere gratitude towards Dr. Andreas Vasdekis, not only for being on my committee but help me understand the complexities of my research work and his willingness to work with me throughout my research work as well. Finally, Dr. Lili Cai to have provided me with her valuable support and guidance throughout my learning process.

Last but not the least, I would like to thank my family for their love and trust, especially my Grandpa for always believing in me, my brother Meetpal for his immense guidance and my friends Paris and Zach for their constant support and encouragement.

Table of Contents

List of Tables

List of Figures

Chapter 1: Introduction and Literature review

1.1 Introduction

The search for alternatives to petroleum based fuels has intensified in the last few decades mainly due to increased energy consumption and the constant decline of crude oil reserves and in regard to the climate change concerns [1]. The rapid growth of human population has seen a sharp increase in the demand for energy, the majority of which comes from petroleum. The bid to keep up the supply of energy with the inexorable fall in the petroleum fuel reserves and the climate concerns have led to the search of alternatives. Some of these include solar power, hydro power, and windy energy, all of which are already being extensively used.

Biofuels have been touted as a promising alternative to conventional fuels where production of fuels such as ethanol from biomass and bio-diesel from plant oils have already been commercialized and put to uses such as transportation [2]. The production of biofuels using microbial biomass has gained traction in the last few decades. Micro-organisms such as bacteria, algae and yeast have the ability to utilize various carbon (C) substrates (e.g. sugars) [3][4][5]. This ability has enabled key research in multiple areas to maximize the efficiency of microbial biofuel production through metabolic engineering.

One such yeast species is *Yarrowia lipolytica*. *Y. lipolytica* is a non-conventional yeast that can be easily found in dairy and meat products and has been well studied regarding its capabilities to produce lipids at an industrial scale [6]. Classified as an oleaginous organism, *Y. lipolytica* can accumulate lipids more than 20% of its cell weight [7] and is able to consume a wide range of C sources [8][9][10]. The yeast is also able to synthesize

triacylglycerol (TAG), also called triglycerides, which can be readily converted to biodiesel at an industrial scale [11], [12]. Another remarkable feature of this yeast is its ability to degrade hydrophobic substances such as n-alkanes, fatty acids, fats and oils, carried out through the presence of its genome of several multigene families involved in specific metabolic pathways [13]. This enables the yeast cells to accumulate lipids to levels >50% of cell weight [12]. Despite of all the recent discoveries, the key target of economic conversion of cellulosic biomass to TAG heavily relies on the proper optimization of microorganisms through metabolic engineering. An essential part of this process is to study the nutrient fate inside the cell such as glucose. One tool that is readily available and studied extensively over the years for single cell imaging and the fate of the nutrients inside a cell has been Raman spectroscopy. [14][15][16][17].

Two common vibrational (Raman and infra-red (IR)) spectral regions between (i) 3000-2800 cm^{-1} and (ii) 1500-1000 cm^{-1} [18] can be used to differentiate the cells without any prior knowledge. In complex biological systems, and cell bodies with extremely low lipid concentration, non-lipid components can also contribute to the scattering in these two spectral regions. Therefore, to identify and monitor the glucose uptake and consumption inside cell a spectral contrast is required.

In this study we aim to synthesize deuterated Raman-probes from the strain MTY038 of the yeast *Y. lipolytica*. The Raman-probe will act as a biomarker and help to track the route of consumption of the glucose as a substrate inside the lipid bodies of the cell and its end fate. This experiment will establish the grounds for the metabolic engineering of the yeast to produce TAGs on an industrial scale.

1.2 Literature Review

1.2.1 *Yarrowia lipolytica*

Yeast are microorganisms that can be found naturally distributed in the natural environment. They are classified as unicellular micro-fungi and more than a 1000 species are known to us, mainly a fraction of their total population on earth [19]. They have continuously been exploited by humans over years and years to produce beer, wine, and bread. The records date back to the Egyptian civilization using yeast for fermentation of alcoholic beverages and bread. *Yarrowia* genus consists of s single species, *Y. lipolytica* commonly found in a number of meat and dairy products[20]. *Yarrowia* genus is a fungus that belongs to the family Dipodascaceae. *Y. lipolytica* has been the core of attention in the past few decades due to a plethora of reasons, one of which is its ability to not only consume but accumulate lipids as well. The ability to accumulate lipids more than 20% of its weight classifies it as an oleaginous microorganism [21].

Y. lipolytica is a non-conventional yeast that can be easily found in dairy and meat products and has been well studied regarding its capabilities to produce lipids at an industrial scale [6]. Classified as an oleaginous organism with the ability to produce lipids in such high quantities, and *Y. lipolytica* is also able to consume a wide range of carbon sources [7] [8][9][10]. Apart from being able to synthesize TAG, which can be readily converted to biodiesel at an industrial scale [12], another remarkable feature of this yeast is its ability to degrade hydrophobic substances such as n-alkanes, fatty acids, fats and oils, carried out through the presence of its genome of several multigene families involved in specific metabolic pathways (Figure 1.2) [13]. This enables the yeast cells to accumulate lipids to levels >50% of cell weight [12].

Figure1.1: *Yarrowia lipolytica* MTYL038 strain grown on a yeast peptone-dextrose gel plate.

1.2.1.1 Physiology

Y. lipolytica is a special purely aerobic yeast that has unique metabolic pathways for the consumption of hydrophobic substrates such as n-alkanes, fatty acids, fats, and oils [22]. The fungus' genome sequence has shown that its closely related to *Saccharomyces cerevisiae*, a very common (brewers and bakers) yeast. The underlying genetic processes, on the other hand, tend to be very distinct, especially the ability of the former to utilize hydrophobic substrates [23]–[25]. When it comes to substrates, *Y. lipolytica* can degrade several hexoses, including glucose, fructose, and mannose. However, some solutes, including sugars, are not freely permeable across cell membranes. Except in cases where a di- or trisaccharide is hydrolyzed outside the cell, transport is the first step in carbohydrate metabolism. Unique transporters, also known as permeases, are responsible for transport across the membrane. In

S. cerevisiae, transport of the typical monosaccharides such as glucose, fructose, or mannose is facilitated diffusion; however, the situation can differ in other yeasts. There is a glucose transport mechanism with two components in *Y. lipolytica*, and their operation is independent of the glucose concentration in the medium [25] [23].

Y. lipolytica can use acetic, lactic, propionic, malic, succinic, citric, and oleic acids as the sole C and energy source, with this ability being independent of the pH of the culture media in most cases as studied by Rodrigues and Pais [26]. When the yeast was grown in glucose and citric or lactic acid, diauxic growth was observed, indicating that the utilization of these two acids is repressed by glucose. The growth of yeast was also inhibited by propionic, butyric, and sorbic acids. The majority of *Y. lipolytica* strains thrive on acetate as their sole C source.

When it comes to the consumption of alcohol, *Y. lipolytica* uses ethanol as a C source at up to 3% concentrations whereas higher concentrations are harmful [27]. In *Y. lipolytica,* several nicotinamide adenine dinucleotides (NAD^+ and $NADP^+$) dependent alcohol dehydrogenases have been discovered. Two NAD^+-dependent alcohol dehydrogenases with different substrate specificities are likely to occur. Both enzymes' synthesis does not seem to be repressed or inducible by glucose or ethanol [28]. Another source that has shown progressive signs of lipid production through *Y. lipolytica* is glycerol. Many yeasts may use glycerol as a C source in aerobic conditions, assimilating it via the glycerol-3-phosphate or dihydroxyacetone pathways [29]. Glycerol is assimilated by several yeasts through dihydroxyacetone. Glycerol dehydrogenase transforms it to dihydroxyacetone, which is then phosphorylated to dihydroxyacetone phosphate by dihydroxyacetone kinase [30]. Raw

glycerol was successfully used by Papanikolaou et al. for *Y. lipolytica* growth and citric acid production [9].

The ability of *Y. lipolytica* to degrade hydrophobic substrates arises from the fact that the yeast is isolated from commonly isolated from lipid-rich environments, such as dairy products, contaminated environments, and raw poultry, and is particularly adapted to hydrophobic substrates. Microorganisms that reside in an aqueous medium with a hydrophobic carbon source, and therefore are distributed in the medium as drops, are thought to have evolved mechanisms to make access to this substrate easier because there is a low risk of interaction between the microorganisms and the continuously moving hydrophobic droplets [22].

1.2.1.2 Metabolite production

Different organic ingredients and minerals used as sources of C, nitrogen (N), and micronutrients, as well as the pH of the growth medium, incubation temperature, inoculum, and oxygenation rate, affect the growth of *Y. lipolytica* and the secretion of metabolites and lipids [22].

Lipase, an enzyme that scientists and industrial researchers are interested in because it can be used in a variety of applications in the detergent, food, pharmaceutical, and environmental industries, is one of the most essential products secreted by *Y. lipolytica* [31]. Another such metabolite known as γ-decalactone, can be produced by bio-transforming ricinoleic acid through *Y. lipolytica* [31]. It is a peach-scented compound that is commonly used in food and beverages, which is why biotechnological processing of it is so appealing

[22]. *Y. lipolytica* churns out a very high yield of γ-decalactone and has many genes encoding hydrophobic substrate degrading enzymes, making it a model for this metabolic pathway. The enzyme that catalyzes the first reaction of oxidation in this sequence belongs to a family of six medium chain acyl-CoA oxidases found in *Y. lipolytica* [32].

When it comes to the production of citric acid, *Y. lipolytica* has been one of the most widely used yeast [33]. As stated by Papanikolaou and Aggelis [10], citric acid is generated primarily when the concentration of N in the culture medium is depleted and sugars or glycerol are used as C sources, according to the author. Nitrogen deficiency induces a rapid drop in adenosine monophosphate (AMP), which is needed for the formation of the intracellular enzyme NAD^+ isocitrate dehydrogenase (which converts isocitric acid to α-ketoglutaric acid), resulting in enzyme activity loss. As a result, when citric acid levels in the mitochondria of the cell reach a critical level, it is secreted into the cytosol. *Y. lipolytica* is the only yeast that can increase citric acid output from both carbohydrate and fat C sources [34]. *Y. lipolytica* has been tested against several C sources for citric acid processing, including glucose [8], n-paraffin [35], ethanol [36], and glycerol [33][34]. The production citric acid in the cell can be highly influenced by both the source of C and its concentration as well [37].

1.2.1.3 Lipid production in *Y. lipolytica*

Microorganisms that are oleaginous have the capacity to convert organic acids into acetyl-CoA, a lipid biosynthesis intermediate [21]. Lipids can be stored within the cell in two ways: (1) *de novo* synthesis, which includes the processing of fatty acid precursors such as acetyl and malonyl-CoA and their incorporation into lipid storage biosynthesis, and (2) *ex*

novo deposition, which involves the capture of fatty acids, oils, and TAG from the growth medium and their accumulation inside the cell. This necessitates the hydrolysis of hydrophobic substrates on the cell's surface, the transport of fatty acids into the cell's interior, and their reassimilation as TAG and esters, accompanied by their accumulation in lipid bodies [12].

The lipid accumulation in *Y. lipolytica* takes place through the *de novo* synthesis involving the production of fatty acid precursors such as Acetyl-CoA and their integration into the Kennedy pathway (Figure 1.2). The glycolysis process inside the cell involves glucose entering the mitochondria as pyruvate. The excess Acetyl-CoA is transported from the mitochondria to the cytosol using the citrate shuttle and gets converted into Malonyl-CoA by Acetyl-CoA Carboxylase (ACC) marking the first step of fatty acid synthesis. The TAG (triglyceride) synthesis follows the Kennedy pathway and takes place inside the endoplasmic reticulum (ER) or the lipid droplets (LDs). Acyl-CoA is the precursor for the formation of lysophosphatidic acid (LPA) which is further acylated to form phosphatidic acid (PA). PA is then dephosphorylated to form diacylglycerol (DAG) and then a final acylation occurs by diacylglycerol acyltransferase (DGA1) to produce TAG [7].

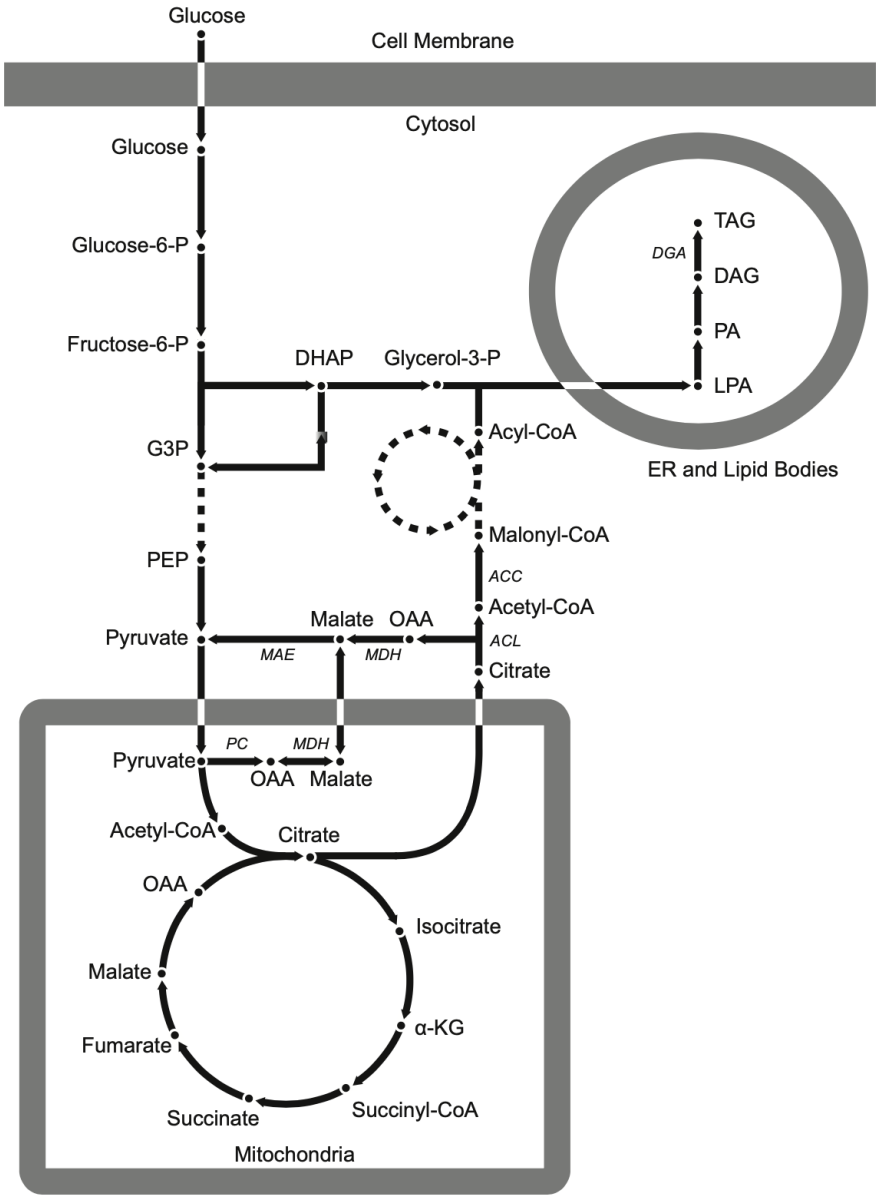

Figure 1.2: Summarized lipid biosynthesis pathway inside *Yarrowia lipolytica [7]*.

The oleaginous organisms began to accumulate lipids when an element in the medium becomes limiting and a C source such as glucose in our case is present in excess [12]. The limiting nutrient in most cases is N as it is the simplest to regulate and the most effective form of limitation for inducing lipid accumulation. The C flux is distributed between the four

macromolecular pools during the growth process (carbohydrate, lipid, nucleic acid, protein). Nitrogen is needed for cellular proliferation since it is required for protein and nucleic acid synthesis. As a result, N deficiency slows this process. However, when N is scarce, the rate of catalytic growth slows significantly, while the rate of C assimilation slows more slowly. As a consequence, C flux is channeled preferentially toward lipid synthesis, resulting in the accumulation of triacylglycerols within distinct lipid bodies in the cells [38] [12].

When there are nitrogen restrictions in the form of ammonium ions in the culture medium and an excess C source such as glucose, microorganisms begin to accumulate lipids [12], [39]–[41]. Several factors during the fermentation process, such as the type of substrate used, the choice of limiting nutrient, temperature, pH, and aeration, influence the fatty acid profiles produced, as well as the volume, productivity, and efficiency of the conversion [39], [42], [43]. The C source has the greatest impact on the lipid composition of yeast-produced oils [8], [33], [43]. The change in C source can lead to a change in the overall lipid yield as well as the composition of the lipids produced as demonstrated through a study where *Y. lipolytica* grown in oleic acid showed an increase in the size of the lipid particles and an overall increase in the lipid production of the cells [44].

1.3 Advances in Metabolic engineering

To covert lipids and TAGs to biodiesel at an industrial scale with prices comparable to petroleum-based fuels, one main aim must be met: metabolic engineering to optimize

microorganisms so that they can economically convert cellulosic biomass to TAG, and thus biodiesel, which often requires genetic manipulations [45].

The optimization of microorganisms faces two broad challenges: (i) the quantity of biofuel precursors produced, as well as productivity, which is measured in production titers per unit time (ii) the proportion of biofuel precursors generated in relation to the amount of substrate consumed. While preliminary attempts have shown promise, engineering lipid biosynthesis pathways in *Y. lipolytica* is still largely unexplored. Beopoulos et al. were able to achieve 40–70% lipids by *ex-novo* lipid accumulation by removing peroxisomal oxidation pathways and engineering glycerol metabolism [46]. Meanwhile the co-expression of Δ6- and Δ12-desaturase genes resulted in substantial γ-linolenic acid development [47].

Stephanopoulos et al. [7] established an expression platform for higher expression using and intron-containing translation elongation factor -1α (TEF) promoter capable of increasing the gene expression 17-fold over the intron-less TEF promoter followed by the overexpression of acetyl-CoA carboxylase (ACC1) and DAG acyltransferase (DGA1), increasing the net yield by 2 and 4 times respectively compared to the parent Po1g strain.

Qiao et al.[48] used a promoter engineering technique in *Y. lipolytica*, replacing the *hp4d* promoter with the *TEFin* promoter to co-overexpress ACC1 and DGA1 as well as the stearoyl-CoA desaturase (SCD). The engineered strain developed a lipid content and titer of 67% and 55 g/L, respectively, in a 1.5-L bioreactor with glucose as the substrate. Furthermore, the engineered strain exhibited a few favorable phenotypes, including rapid growth, high sugar tolerance, and a high content of unsaturated fatty acids.

Xiong et al. [49] have tweaked the intracellular lipid metabolism in *Y. lipolytica* in this study to generate fatty acids. To minimize fatty acid consumption by the native pathways in *Y. lipolytica*, two key strategies were used: blocking activation and peroxisomal absorption of fatty acids and eliminating lipid biosynthesis. Fatty acid development was increased by both genetic modifications. The thioesterase gene *tesA* from *Escherichia coli* was expressed in the strain with disrupted *faa* genes encoding fatty acyl-CoA synthetases and pxa1 encoding peroxisomal acyl-CoA transporter, and the fatty acid titer resulted an 11-fold increase over the parent strain.

Apart from optimizing the lipid yields a plethora of studies have been performed on *Y. lipolytica* such as the engineering of unconventional yeast for efficient succinic acid production from glycerol [50]. Another important secondary plant metabolite resveratrol has been extensively studied over the past two decades due to its ability to be used as a food supplement as well as being beneficial to treat diseases such as diabetes and neurological disorders. Borodina et al. [51] have engineered *Y. lipolytica* strain to improve its resveratrol production capabilities by 8 times.

But the question at stake is to explore the capabilities of *Y. lipolytica* to optimize the lipid production inside the cell. An essential part of the process is to study the consumption and nutrient fate inside the cell of a substrate such as glucose. One tool that is readily available and studied extensively over the years for single cell imaging and the fate of the nutrients inside a cell has been Raman spectroscopy.

1.4 Raman Spectroscopy

Raman spectroscopy is a cutting-edge cell imaging technique that overcomes some of the drawbacks of existing methods. Raman spectroscopy is a technique based on the detection of a scattered laser light from a sample. Raman differentiates itself from other forms of imaging as its scattering effect is unique for different molecular structures. It is a fast technique that can be done in aqueous systems (e.g. biological) and is non-destructive and is been used to study single cell organisms [17] [52][53][54].

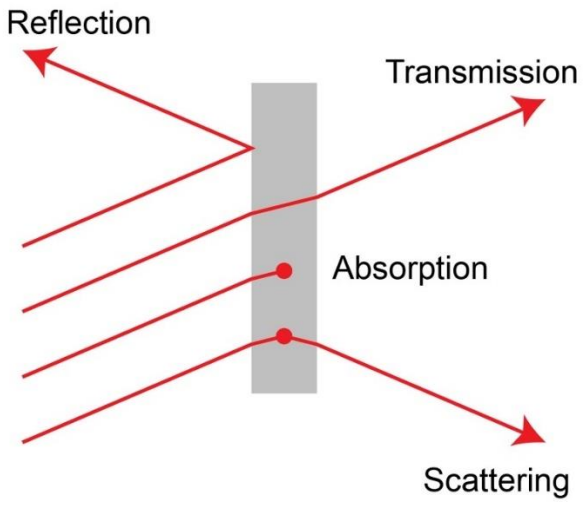

Figure 1.3: The basics of measurement of light

The methodology of Raman Spectroscopy entails shining a monochromatic light source (such as a laser) on a sample and measuring the scattered light (Figure 1.3). Most of the dispersed light would pass through the sample untouched. Rayleigh or elastic scattering occurs because of the detector receiving energy with the same frequency as the excitation

source. A very small amount of scattered light (1 in 10^7) has its energy transferred away from the laser frequency, known as the Raman or Stokes shift. Since the anti-Stokes-shifted Raman energy is weaker than the Stokes-shifted energy at room temperature, it is normally ignored and filtered out. This is due to interactions between the incident electromagnetic waves and the molecules' vibrational energy levels. In other words, the interaction can be interpreted as a change in the electric field of the molecule (Figure 1.4).

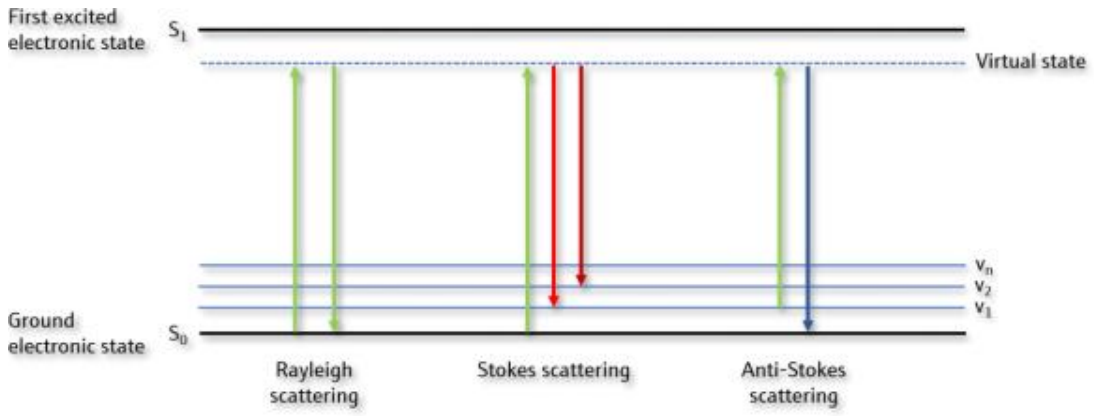

Figure 1.4: Rayleigh scattering (no interaction) and Stokes's shift (interaction) are energy differences between incident and scattered photons described by arrows of different lengths at the molecular energy level.

Intramolecular vibrations are not the only thing that Raman spectroscopy can detect. Raman-active motions include crystal lattice movements and other prolonged solid motions. In fields including geochemistry and mineralogy, their spectra are crucial. The electromagnetic field interactions within the molecule's bonds can easily illustrate Raman selection laws. As shown in Equation 1, the dipole moment, P, caused in a molecule by an external electric field, E, is proportional to the field.

$$P=\alpha E \qquad \text{(Equation 1)}$$

The polarizability of the molecule is the proportionality constant, denoted by α. The polarizability of an electron cloud around a molecule is a calculation of how quickly it can be skewed. In simpler words, the polarizability of an electron cloud is an indicator of how easily it can be bent by an electric field. The electron cloud is usually associated with an atom, molecule, or ion. An electrode or a nearby cation or anion could be the source of the electric field. If the degree of polarization is quite small, an ionic bond is formed, while if the degree of polarization is large, a covalent bond is the result**.** The species to which an electron cloud belongs is said to be polarizable if it is simple to distort. The induced dipole emits or scatters light at the incident light wave's optical frequency. Raman scattering is caused by a change in the polarizability of the bond. The square of the induced dipole moment determines the scattering intensity.

If a vibration has no effect on polarizability, the polarizability derivative will be close to zero, and the Raman band strength will be low. A strongly polar moiety, such as the O-H bond, normally has weak vibrations. A large change in the dipole moment cannot be caused by an external electric field, and stretching or bending the bond has no effect, resulting in a weak or non-Raman signal. Moieties with scattered electron clouds or high polarizability, such as carbon-carbon double bonds, are typical strong Raman scatterers. In an external electric field, the double bond's π-electron cloud is quickly skewed. The distribution of electron density changes dramatically as the bond is bent or stretched, resulting in a significant change in the induced dipole moment.

The incident photon energy will excite vibrational modes of polarizable molecules, resulting in scattered photons that are depleted in energy by the sum of vibrational transition

energies, giving rise to the Raman peaks. The number of peaks in a molecule is equal to the number of degrees of freedom it has (Figure 1.5).

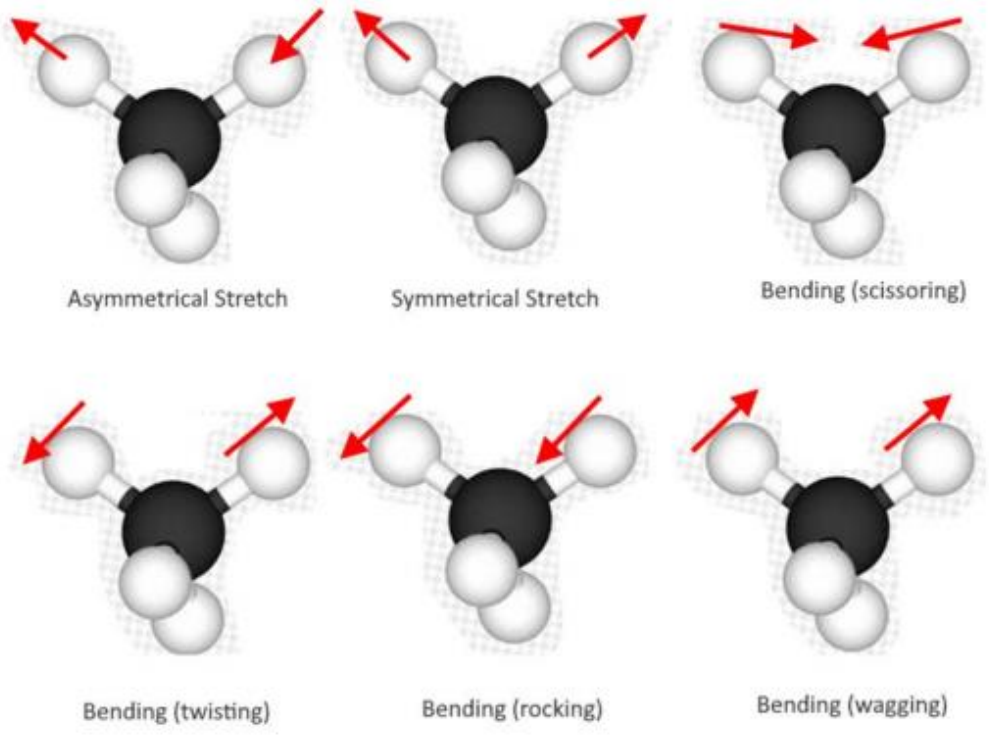

Figure 1.5: A visual representation of the types of vibrations induced in a molecule because of the incident light.

1.4.1 Raman/FTIR spectroscopy of biomolecules

The cell is the fundamental biological unit of all living organisms, and understanding cellular dynamics and processes is important for biological research. The studies are not only limited to human body but extend to a wide variety of biological macromolecules as well. The application of Raman spectroscopy in the analysis of biomolecules is becoming an immense

force to break down the barriers in the identification, analysis, and optimization of biological cells and materials [55], [56].

For Fourier transform infra-red (FTIR) and Raman spectroscopies, two common spectral regions between (i) 3000-2800cm^{-1} and (ii) 1500-1000cm^{-1} [18] can be used to differentiate between the cells without any prior knowledge, containing the rich and innate information regarding a cell. A single cell Raman spectrum can provide a wide array of vibrational bands associated with proteins, lipids, and polysaccharides (Figure 1.6) [57], [58].

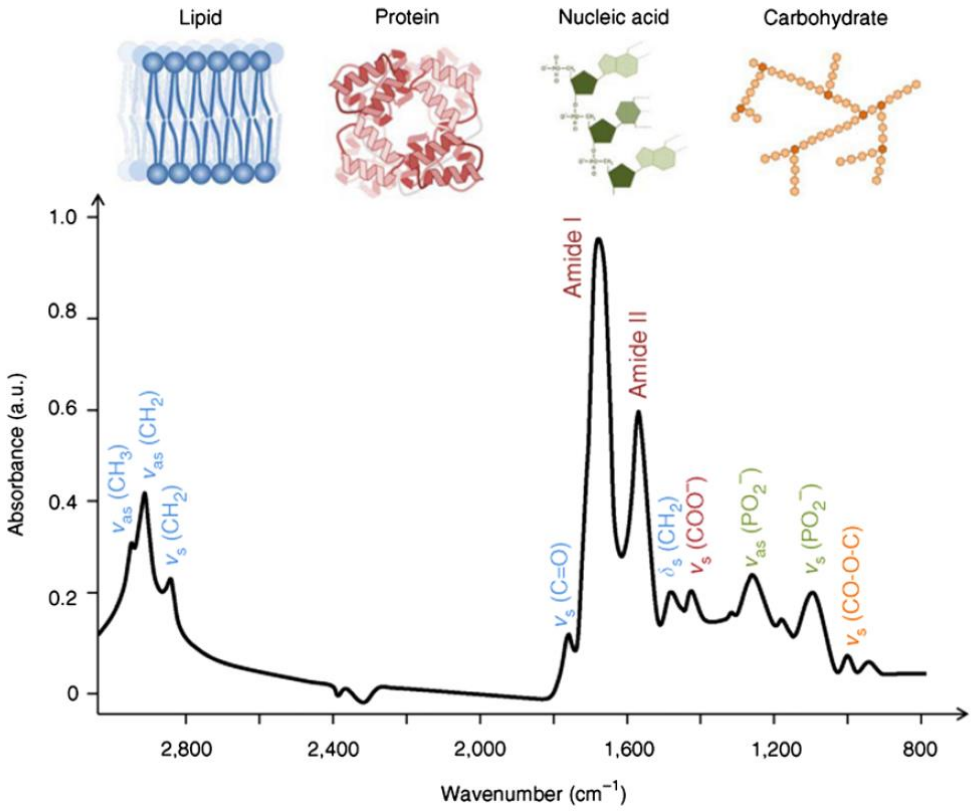

Figure 1.6: FTIR spectrum of common biomolecules [58]

Lipids are one of the most important groups of biomolecules involved in cellular signaling, energy storage, and membrane formation. The existence of long non-polar acyl chains in the structures of many lipids results in a broad Raman scattering cross-section. As a result, lipid

bands are ubiquitous in the Raman spectra of cells and tissues, and in many instances, they act as useful pathology markers [59].

The presence of the hydrocarbon chain is the most distinguishing attribute of lipid Raman spectra, which can be found in the three following regions: 1500–1400, 1300–1250, and 1200–1050 cm^{-1}. Scissoring and twisting vibrations of the CH_2 and CH_3 groups are assigned to the bands 1500–1400 cm^{-1} and 1300 cm^{-1}, respectively. The C–C stretching vibrations are responsible for bands in the 1200–1050 cm^{-1} region. Another characteristic feature of lipid spectra is a very intense group of bands in the higher wavenumber range (3100–2800 cm^{-1}) caused by C–H stretching modes [60].

1.4.2 Stimulated Raman Scattering (SRS)

Raman spectroscopy is a valuable instrument for evaluating organic molecules based on vibrational frequencies, and it perfectly complements infrared spectroscopy. Raman-probes have emerged as a better alternative to fluorescent labels. These probes, unlike fluorescent labels, are unaffected by photobleaching, allowing for long-term cell imaging. More significantly, Raman active modes have a spatial extent of just one or a few chemical bonds, which is much smaller than the chemical structure of fluorescent moieties. Raman labels can be selected from endogenous compound spectral signatures or chemically modified probes that improve Raman response and selectivity. This notion has given rise to technologies such as simulated Raman scattering (SRS) [61], [62].

Raman spectroscopy uses inelastic photon scattering to classify molecular vibrations and thus provides information on the concentration and structure of chemical bonds within a

specimen. The characteristic chemical moieties of different types of molecules, such as CH_2 for lipid and amide or CH_3 for protein, may be used to identify them. Raman (micro)spectroscopy, also, relies on weak spontaneous scattering and is thus unsuitable for high-speed imaging. In SRS microscopy, detection, sensitivity, and imaging speed are all greatly improved [63]–[66]. SRS works by using two coordinated pulsed lasers (usually in the near infrared or visible range) to generate a beating field at their different frequencies, which selectively accelerates the matching molecular vibrational transition by up to 10^8 times. After light–molecule interaction, the intensity shift of the incident beams (also known as stimulated Raman loss or gain) is proportional to the analyte concentration, while the quadratic laser power dependency allows for three-dimensional optical sectioning. By changing the laser wavelength, a stack of hyperspectral images (at selected frequencies) can be obtained. By collecting images at off-peak frequency, non-vibrational-resonance history can be subtracted [67].

1.5 Raman monitoring of metabolites and substrates

Raman spectroscopy has made important progress in monitoring the glucose fermentation reaction in yeast over the last 30 years. Shope et al. [68] studied the reaction mechanism of yeast fermentation in the late 1980s and commented on its limitations. Shaw et al. [69] used Raman spectroscopy to track a fermentation phase and were able to assess the concentrations of glucose and ethanol after particulate matter was extracted by filtration in a by-pass.

When it comes to the applications of FTIR/Raman, both the technologies have a specific set of advantages and disadvantages. Sivakesava et al. [70] used both FTIR and FT-Raman spectroscopies to simultaneously monitor ethanol, glucose, and optical cell density, but Raman spectroscopy was less accurate at low concentrations than FTIR spectroscopy due to weak scattering. The absorption of water in the mid-IR region is very heavy, as its OH-bending absorption is much greater than any signal from the rest of the biomolecules in the samples. This is a major drawback of IR. To achieve acceptable signal-to-noise ratios (S/R), this problem can be partially overcome by dehydrating the samples or, in the solution, by subtracting the water signal, restricting the path lengths to 10 μm, and using relatively high concentrations (>20 mg mL^{-1}) of biomolecules. FTIR also suffers from low sensitivity in thin samples such as monolayers because of Beer-Lambert's Law [71]. This limitation can be overcome by a strong signal amplification based on the plasmonic resonances present in nanoscale metallic particles, resulting in the phenomenon of surface-enhanced infrared absorption. Another alternative is the attenuated total reflectance (ATR) focusing on aqueous biological samples.

Unless improved Raman scattering processes are used, the Raman efficiency is very poor when compared to the FTIR. In fact, the spontaneous Raman signal is inherently weak because only one out of every 10^7 photons undergo inelastic scattering, resulting in Raman cross-sections (1029–1030 cm^2) that are significantly lower than fluorophores' normal absorption cross-sections (1015–1016 cm^2). As a result, Raman spectra acquisition times can be very long. Furthermore, the Raman spectra of biological samples obtained with a visible laser can be dominated by a very large fluorescence background, which must be mathematically extracted before the sharp Raman peaks can be observed [71].

Advances in noninvasive glucose measurements have been widely used in studies such as Berger et al. [72], who used near-infrared Raman spectroscopy to assess glucose concentrations in human blood samples, and Enejder et al. [73], who investigated glucose levels in transcutaneous blood. Bechtel et al. [74] used intrinsic Raman spectroscopy in conjunction with various statistical methods to boost prediction errors on physical tissue models, reducing errors caused by absorption and scattering effects during transcutaneous measurements.

For the optimization of ethanol production from the yeast *S. cerevisiae,* Hirsch et al. [75] have developed a noninvasive inline Raman monitoring and feedback control of glucose concentration during ethanol fermentation. By Raman spectroscopy-based feedback control, the glucose concentration was maintained at 100 g/L by the automatic feeding of concentrated glucose solution. The control of glucose concentration during fed-batch fermentation resulted in increased ethanol production. Ethanol yield of 86% was achieved compared to the batch fermentation when 75% yield was obtained.

Schalk et al. [76] designed a large-aperture Raman probe to avoid potential sterilization issues and biofilm formation on the probe tip of a commercial spectroscopic equipment. The probe's architecture allows for noncontact in-line measurements of bioreactors and chemical reactors through glass vessels or inspection glasses. During yeast fermentation, the probe's functional applicability was checked by tracking the consumption of substrate glucose and the formation of ethanol as a commodity.

Depending on cultivation conditions and environmental stress, the yeast *Metschnikowia* can be considered an industrially viable source of pulcherrimin (an iron chelate) or single-cell lipids. Raman spectroscopy was used to successfully distinguish both

pulcherrimin and lipids in single yeast cells in a study by Nemcova et al. [77]. According to the findings, pulcherrimin output is strongly influenced by ferric ion concentration, with the highest yield in media containing 0.1 g/L iron. Furthermore, the synthesis of lipids in *Metschnikowia* cells was investigated at various temperatures and C:N ratios, using Raman spectroscopy to track the composition of fatty acids under various conditions, as well as monitoring the iodine amount. The Raman spectroscopy findings were comparable to the gas chromatography fatty acid study.

The use of Raman profiling is not limited to a particular set of microorganisms. Huawen et al. [78] have described a method or direct, quantitative, *in vivo* lipid profiling of oil-producing microalgae using single-cell laser-trapping Raman spectroscopy, yield a real-time chemical information in a label-free manner, eliminating the limitations of impermeability, toxicity, and specificity of the fluorescent probes common in many other used protocols.

1.6 Microorganisms in a deuterated environment

Harold Urey [79] who received the Nobel Prize for his discovery in 1934, was the first to discover deuterium (D), a hydrogen (H) isotope with an atomic mass of two. Deuterium's nucleus contains not only a single proton, as is the case with the more familiar hydrogen isotope, protium, but also one neutron. This small yet important difference is the basis of deuterium's unusual properties, which have piqued the scientific community's interest for nearly 90 years. Deuterium's special properties indicated that it would have a major effect on biological systems. Numerous physiological processes, as well as the anatomy of affected

cells or organisms, are altered or completely disrupted by deuteration. Some of these effects are complex, while others are straightforward, such as D_2O's (heavy water) reduced ability to dissolve certain biomolecules. Less soluble carbohydrates, such as maltose or raffinose, are more affected by the lower solubility, whereas well soluble saccharides, such as glucose, maltose, or xylose, are unaffected [80]. In D_2O, polypeptides become more stable, reducing the surface area in contact with the solvent by adopting a more compact globular form or associating into larger aggregates [81].

The kinetic isotope effect (KIE) occurs when chemical reactions with the same atoms, but different stable isotopes have different reaction rates. This impact is very poor for most biogenic elements [82]. Because of the large difference in atomic mass and nuclear spin between protium and deuterium, the KIE is the highest in H isotopes. D reacts much more slowly than H in chemical and biochemical reactions because D-C bonds have a lower zero-point energy (lowest ground-state vibrational level) than H-C bonds [83]. The amount of energy required to activate the molecule to its transition state increases as the zero-point energy decreases. As a result, substituting D for H in chemical bonds changes the rate of bond cleavage and the relative rate of chemical reactions significantly.

Various bacteria, such as *Escherichia coli* [84] and *Bacillus subtilis* [85], as well as fungi, such as *Aspergillus niger* [84], can live in completely deuterated medium. Many cyanobacteria grew in high D_2O concentrations, according to Crespi et al. [84]. Their growth was, however, slower and followed by morphological anomalies such as discoloration, cell enlargement, and clump formation. Chorney et al. [86] cultivated the unicellular green algae *Scenedesmus obliquus*, *Chlorella vulgaris* and *ellipsoidea* in a nearly pure D_2O medium and found a gradual rise in the lag time and a decline in maximum growth rate. The density of

cells achieved by the culture. Furthermore, they found when transferred to D_2O, the appearance of massive "monster" cells because of stifled division. After a few more days of cultivation, both plants were ready to harvest as they adapted and eventually divided in their new environment.

Various other studies have shown a noticeable delay in cell division when the cells are grown in a deuterated environment [83]. One such study dating back to 1934, where Richards et al. describes the changes in the cell physiology after the growth of the yeast *S. cerevisiae* in D_2O [87]. Richards observed that the total volume of cells from the population grown in D_2O is greater than that from the control population. The difference tends to increase with the age of population. The dry weight of the yeast also sees an increase when the cells are grown in the deuterated media.

The production of perdeuterated lipids from yeast grown in a deuterated environment has not been studied rigorously enough in the past due to several challenges such as the complexity of working on isotope labelled compounds and the input cost required to generate a perdeuterated media for cell growth. Ghellinck et al. [88] have shown that with a deuterated growth environment, a change in the growth period for the cells of *Pichia pastoris* is observed followed by a change in the unsaturation level. *Pichia pastoris* is well known to produce polyunsaturated fatty acids such as linoleic acid (C18:2). The increased production of oleic acid (C18:1) when the cells are grown in a perdeuterated environment comes from two factors: the regulation of yeast to maintain the membrane fluidity and the KIE. The kinetic isotope in this case consists in replacing a CH_2 by a CD_2 unit in different positions in the fatty acid chain and measuring the kinetics of the desaturation process.

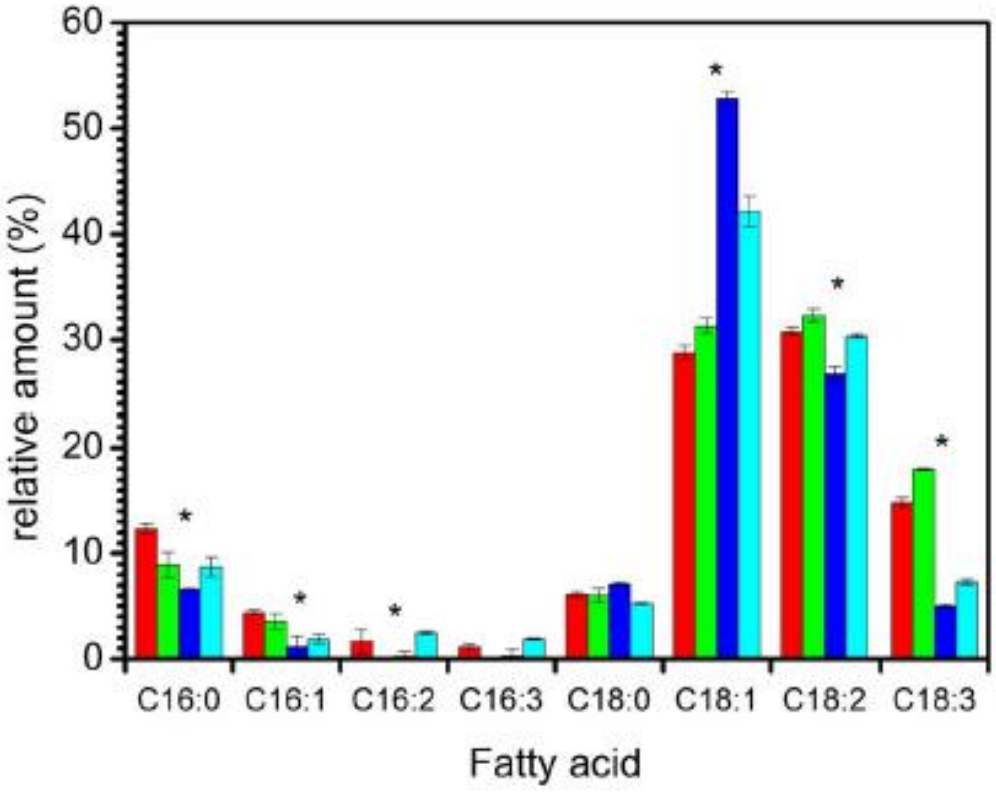

Figure 1.7. Total fatty acid distribution in *Pichia pastoris* cells grown in a hydrogenated environment at 30° C (red) and 18° C (green) and in a deuterated environment at 30° C (blue) and 18° C (cyan). Notice that the amount of polyunsaturated fatty acid shows a decrease when the cells are grown in a deuterated media while unsaturated fatty acids show a growth [88].

1.7 Isotope-labelled Raman-probes

Raman-markers/probes are the single most important precursor when it comes to single-cell Raman micro-spectroscopy. A single-cell Raman spectrum (SCRS) can be thought of as a cell's biochemical fingerprint, revealing details such as basic biomolecules, unique biomarkers, and metabolic states [89], [90], [91]. Raman spectroscopy combined with deuterium isotope probing (Raman–DIP) can be used to investigate single cell metabolism *in situ* [92], [93]. Labels based on stable isotopes, such as D, are often used in clinical settings.

Deuterated substances are commonly used in clinical trials aimed at researching the absorption and movement of drugs in humans since the level of toxicity of pharmacological substances and their deuterated analogs is normally similar [94].

Berry et al. [93] have grown bacteria in D_2O and using this approach they characterized the activity patterns of two dominant microbes in mouse cecum samples amended with different carbohydrates and discovered previously unidentified bacteria stimulated by mucin and/or glucosamine by combining Raman micro-spectroscopy and optical tweezer-based sorting. In another study by Xu et al. [91], the authors have found a distinguishable C-D vibration band at 2070-2300 cm^{-1} in SCRS when *Escherichia coli* used deuterated glucose and *Pseudomonas sp.* used deuterated naphthalene as sole carbon sources. The intensity of the C-D band is proportional to the extent of deuteration in the carbon source, and as little as 5% deuteration can be distinguished by analysis of SCRS.

SCRS is not restricted to biological microorganisms only. Manen et al. [92] used a combination of nonresonant Raman microspectroscopy and spectral imaging, as well as stable isotope labeling by amino acids in cell culture (SILAC-stable isotopic labeling by amino acids in cell culture), to detect deuterium-labeled phenylalanine, tyrosine, and methionine incorporation into proteins in intact, single HeLa cells. These amino acids have C-D stretching vibrational bands in the 2100-2300 cm^{-1} spectral region, which is free of vibrational contributions from other nondeuterated intracellular constituents. The level of isotope incorporation into the proteins increased with the incubation time.

In complex biological systems, and cell bodies with extremely low metabolite concentrations, non-metabolite components can also contribute to the scattering in between the spectral regions. Therefore, to identify and monitor the uptake and consumption of a

specific substrate inside cell, a spectral contrast is required. As explained by Zhang et al. [67] glucose-D_7 is a promising metabolic probe of macromolecule synthesis for SRS microscopy. In the experiments Zhang et al. have discussed the Raman spectra of cells cultured in glucose-D_7 based media. In the cell-silent area (1,800–2,600 cm^{-1}), glucose-D_7 substituted medium revealed a band at 2,150 cm^{-1}, confirming the formation of C–D bonds in cell molecules, enabling them to image the glucose metabolism in mouse tissues including tumors, brain, intestine and liver.

Garcia et al. [95] have successfully generated a highly deuterated cholesterol (D_{38}-cholesterol) through a yeast strain grown in 99.8% D_2O. This enabled them to detect signals produced by the D_{38}-cholesterol using SRS and perform the selective imaging of cholesterol storage in the mammalian cells. The gas chromatography-mass spectrometry (GCMS) traces of D_{38}-cholesterol and natural cholesterol were observed to be similar with the only change being a slight reduction in the retention time of D_{38}-cholesterol. The Raman spectra of D_{38}-cholesterol showed a Raman shift in the Raman silent region. Commercially available D_7-cholesterol was put up against its D_{38} counterpart and the changes in the C-D and C-H stretches were observed through Raman spectroscopy (Figure 1.7).

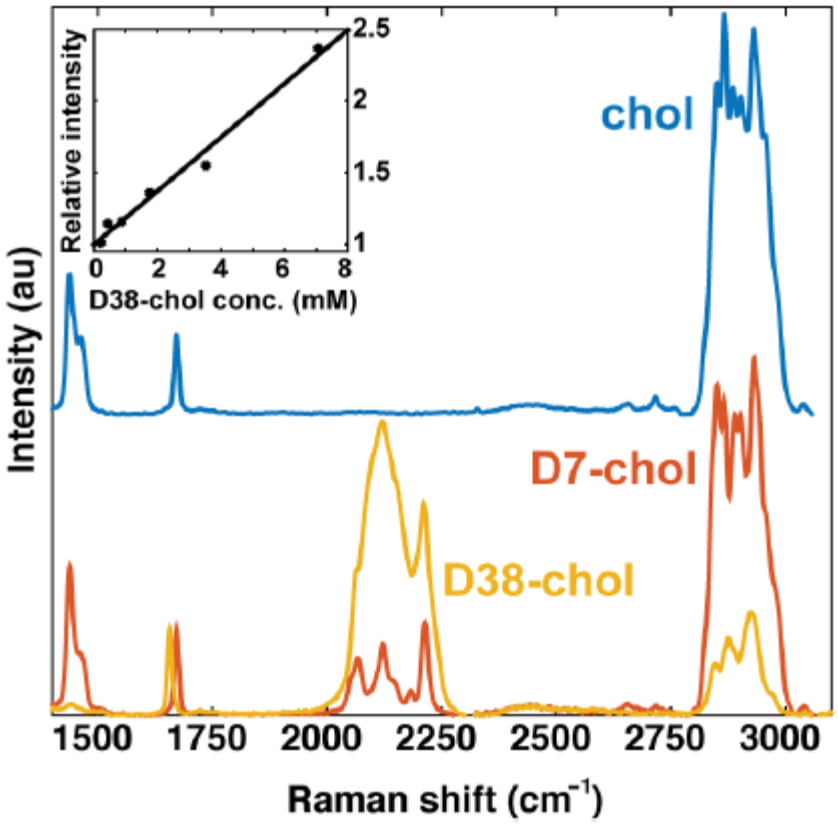

Figure 1.8: Raman spectra of cholesterol, D_{38}-cholesterol, and D_7-cholesterol [95].

In another similar study Xu et al. [91] found distinguishable C-D vibration band at 2070-2300cm^{-1} in a SCRS when *E. coli* and *Pseudomonas putida* were grown using used glucose-D_{12} and D_8-naphthalene as sole carbon sources (Figure 1.8). The intensity of the C-D bands was observed to be directly proportional to the extent of deuteration of the carbon source. Another interesting observation was made that the lipid conversion rate of D_8-naphthalene was lowered compared to glucose-D_{12} and an implication of different anabolic pathways and membrane alteration.

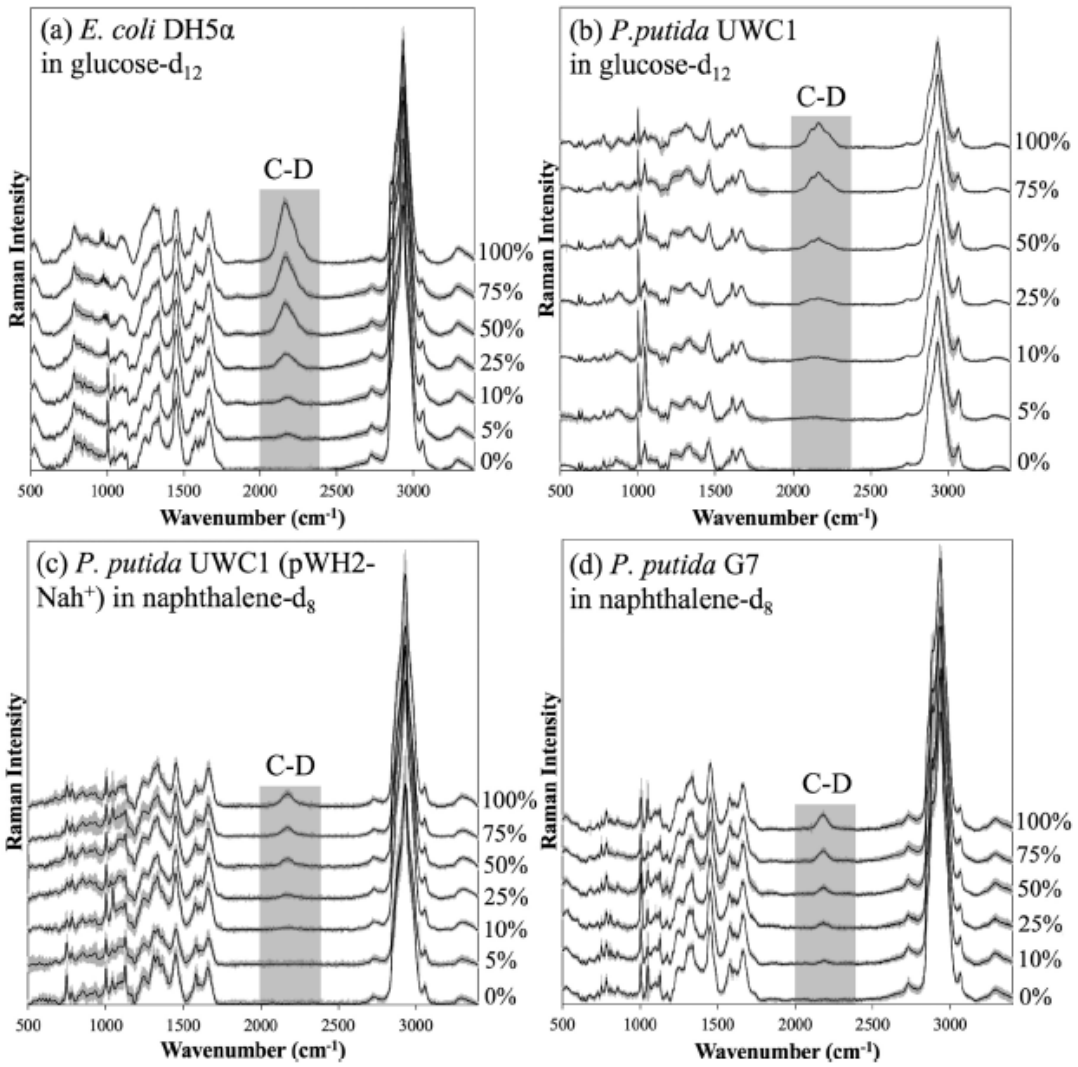

Figure 1.9: Single-cell Raman spectra (SCRS) of (a) *E. coli* DH5α and (b) *P. putida* UWC1 grown in glucose with different ratios of glucose-D_{12} and of (c) *P. putida* UWC1 (pWH2-Nah+) and (d) *P. putida* G7 grown in naphthalene with different ratios of D_8-naphthalene. The characteristic C−D Raman band centered at 2170 cm^{-1} is highlighted; it increases in intensity with increasing deuteration of the carbon source in all cases [91].

Buchy et al. [96] have paved the way to successfully obtain a deuterated probe for the confocal Raman microscopy imaging of *squalenyol* nanomedicines. The Shapiro reaction of the sulfonylhydrazone of acetone-D_6 with an ω-silyloxysqualene aldehyde derivative, accompanied by a regioselective reduction of the obtained allylic alcohol, was used to create squalenic acid-D_6 with a 0.6% yield. The deuterated conjugate was created by coupling the

synthesized to gemcitabine (gem). The Raman spectra of the nano assemblies of this conjugate were recorded showing significant Raman peaks in the silent region of the cells (Figure 1.10).

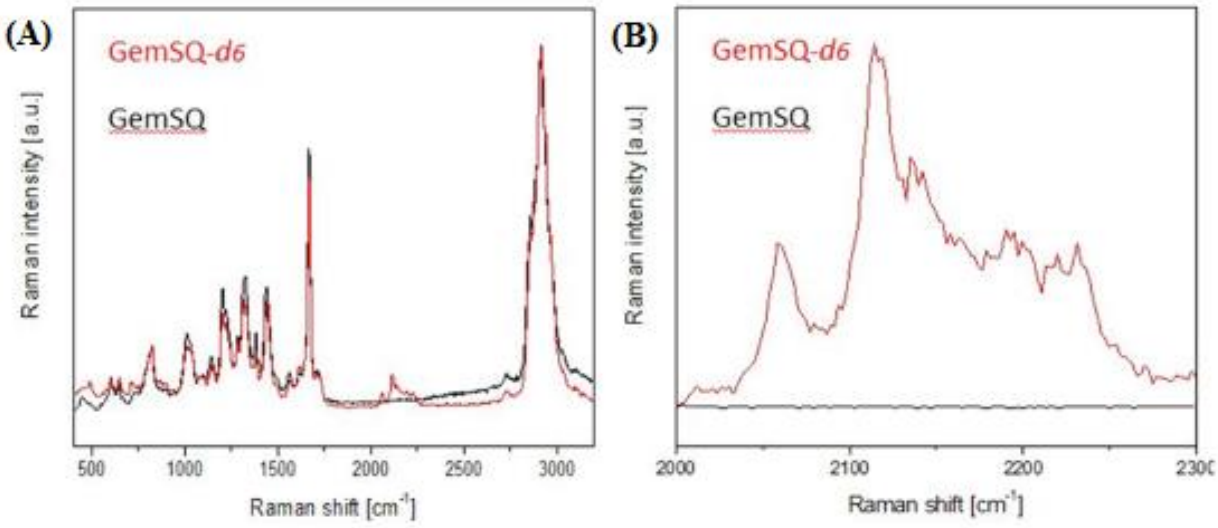

Figure 1.10 (A) Single Raman spectra of deuterated GemSQ-D_6 NAs (red) and GemSQ NAs (black). (B) Close-up showing the difference between deuterated and non-deuterated compounds.

1.8 Research Objectives

The aim of this study is to introduce deuterium tags into the biosynthesized TAG in *Y. lipolytica* which is fed deuterium-labelled glucose (glucose-D_7) media in H_2O or D_2O. Non-deuterated glucose in H_2O was used as a control. The labeled/non-labelled cells were subsequently studied by Raman and FTIR spectroscopies and microscopy. The extracted lipids were analyzed by (i) FTIR and Raman spectroscopies, (ii) by GCMS as their fatty acid methyl ester (FAME) derivatives, and (iii) electrospray ionization-mass spectrometry. The residue left after the extraction of lipids from the biomass was analyzed for sugar composition as their alditol acetate derivatives by GCMS to determine the extent of cell wall component deuteration inside the cell.

These objectives will help us clarify the uptake and consumption of glucose inside a yeast cell., The GCMS and ESI-MS can help us outline the lipid yields and profiles of the biomass grown in different substrates and the effects of the substrates on the composition of lipids as well. The difference between the lipid production capacities of the yeast can be analyzed. Through the intensities of the C-D and C-H in the Raman and FTIR spectra, the amount of glucose substrate utilized inside the yeast cell or for the formation of the cell wall and for the formation of lipid bodies can be determined.

Chapter 2: Materials and Methods

2.1 Cell Culture and Growth

The *Y. lipolytica* strain, MTYL038 was grown using two different media namely yeast peptone-dextrose (YPD) for cell proliferation and yeast synthetic media (YSM) for lipid production. The cells were first grown on a YPD gel plate (10g/L yeast extract, 20g/L of peptone, 20g/L of glucose, 20g/L of agar). For cell culture the YPD also known as the rich media was used (10 g/L yeast extract, 10g/L peptone, 20 g/L glucose). The YSM media consisted of 1.7 g/L yeast nitrogen base (BD Difco, DF0335-15-9), 20 g/L of glucose and water to 90% of the anticipated volume. The strains were first grown on the YPD gel plate for 24 h and transferred to a test tube containing 5 mL YPD medium and incubated at 28ºC for 24 h on an incubator-shaker. The optical density was monitored at 640 nm on a UV-VIS spectrophotometer (VWR V-1200). The cells were transferred to a fresh tube containing 5 mL YPD media and incubated for 24 h at 50x dilution. The cells were taken out, centrifuged, and washed with YSM solution 3 times before being transferred to a tube containing 10 mL YSM media and incubated for 96-100 h.

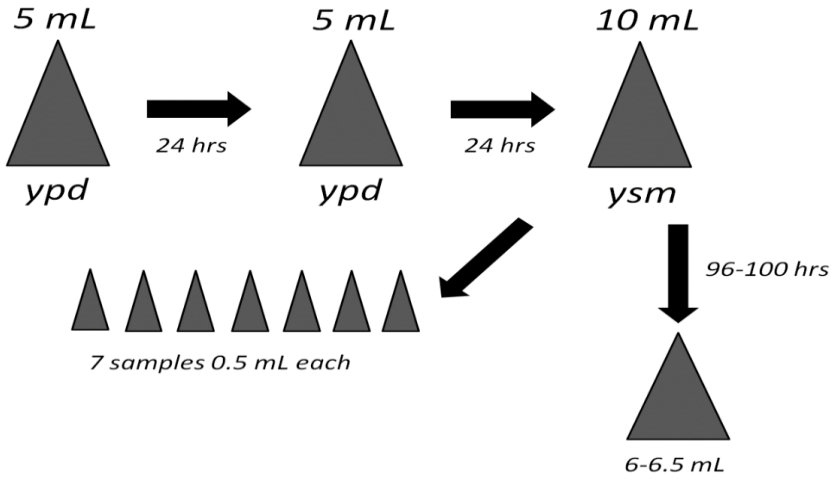

Figure 2.1: Workflow chart for culturing *Y. lipolytica* and sampling.

The YSM recipe was prepared using three different feed substrates: (i) glucose in water, (ii) glucose-D_7 (D-Glucose-1,2,3,4,5,6,6-D_7, 97-98%, Cambridge Isotope Laboratories) in water, and (iii) glucose-D_7 in D_2O (99.8%, Acros Organics). The cultures were each grown in triplicate using each of the YSM recipes. Glucose consumption was monitored during the lipid production stage by taking a 50 µL aliquot and diluted to 1 mL at 7-time intervals, filtered 0.45 µm nylon, and analyzed by HPLC with refractive index detection (SE-61, Shodex) using a Rezex ROA organic acid column (7.8 mm x 300 mm, Phenomenex) at 65ºC on elution with 0.01M H_2SO_4. The remaining yeast cells were centrifuged, washed with water, recentrifuged and then freeze dried (Labconco Freezezone)(Figure 2.1).

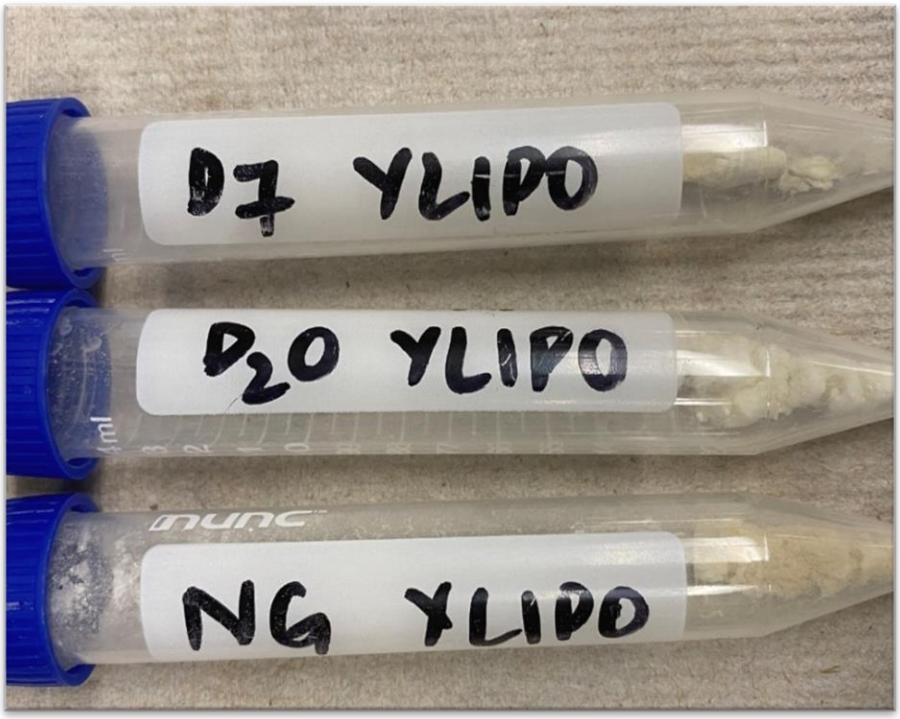

Figure 2.2: *Yarrowia lipolytica* biomass after freeze drying for 48 h.

2.2 Lipid Characterization

Biomass and extract samples (2 mg) were heated in a sealed 5 mL reacti-vial™ for 90 min at 90 °C in a mixture of $CH_3OH/H_2SO_4/CHCl_3$ (1.7:0.3:2.0 v/v/v, 2 mL) to convert to their FAME derivatives. $CHCl_3$ contained 1-naphthaleneacetic acid was used as an internal standard (240 μg mL^{-1}). Water was then added, vigorous mixed, and the organic layer recovered and dried over anhydrous sodium sulfate. The FAME compounds were analyzed by GC–MS on an ISQ-Trace1300 instrument (ThermoScientific) equipped with a ZB-5 (30 m x 0.25 mmØ, Phenomenex) capillary column and temperature program of 40 ºC (1 min) to 250ºC (10 min) at the rate of 5 °C min^{-1}. The eluted compounds were identified with authentic saturated and unsaturated C_{12} to C_{24} fatty acid standards, palmitic acid-D_{31} (98%, Cambridge Isotope Laboratories) standard, and by spectral matching with the 2017 NIST mass spectral library. Lipids were extracted from the biomass (40 mg) with $CHCl_3$ (10 mL) under constant shaking for 12-18 h, then sonicated for 1 min, the extract recovered and evaporated to dryness, and yield recorded. The lipid extracts were analyzed as their FAME derivatives, as described above. The extracted lipids (1 mg in 1 mL of 50:49:1 $CH_3OH/CHCl_3/CH_3COOH$) were analyzed directly for TAG by the positive ion electrospray ionization-mass spectrometry (ESI-MS) on an LCQ-Deca instrument (ThermoQuest) between *m/z* 100–2,000.

2.3 Carbohydrate analysis

The carbohydrate analysis on the extractive free residues (1 mg) and hydrolyzed in 2M trifluoracetic acid at 100ºC for 4 h, then evaporated to dryness. To the hydrolyzed samples,

glucose (0.4 mg), glucose-D_7 (0.4 mg), mannose (0.4 mg) and galactose (0.4 mg) standards, inositol (0.05 mg) was added as an internal standard, samples then reduced with sodium borohydride, acetylated with acetic anhydride to form alditol acetate derivatives and were analyzed by GCMS (ISQ-Trace1300,ThermoScientific) equipped with a BPX70 (30 m x 0.25 mmØ, SGE) capillary column and temperature program of 190 ºC (1 min) to 250ºC (20 min) at the rate of 2 °C min^{-1}) [97].

3.3 Spectroscopy and microscopy

FTIR spectra (in triplicate) was obtained for each dried biomass sample, lipid extracts, and extracted biomass residues using a Thermo-Nicolet iS5 spectrometer equipped with a ZnSe attenuated total reflection (iD5 ATR) accessory with a total of 64 scans per sample. The spectra were baseline corrected and averaged using the Omnic v9 software (Thermo-Nicolet). Raman spectra (in triplicate) for biomass, extracts, and extracted biomass residue samples were obtained using a Witec Alpha 300R microscope-spectrometer with 532 nm laser excitation with a 1 s acquisition time. The spectra were recorded as Grams/32 (*.spc) files, averaged and baseline corrected using the Omnic v9 software. The dried biomass, 4-5 mg was suspended in 1 mL phosphate-buffered saline (PBS) solution and sonicated to break up the coagulated cells.

3.4 Cell imaging

The cells were observed under a Leica DMi8 optical microscope at 100x, with a Leica lens of NA 1.35 oil immersion objective with PH3 and a NA 0.5 illumination condenser. The scope for the microscope is an inverted Leica DMi8. A total of 100 images were taken per sample using the Basler cameras with a pixel size of 1.85 μm and analyzed for their morphology (diameter) using ImageJ software. The analysis was performed by adjusting a local thresholding algorithm for each image.

3. Results and Discussion

3.1 Cell growth and lipid analysis

3.1.1 Biomass yield

Y. Lipolytica cells were proliferated using the YPD media and an optical density of 2.6 was obtained after 24 h for each sample before being transferred to the synthetic YSM media. The glucose concentration in the YSM culture media was monitored over 96 h (Figure 3.1). For the glucose - H_2O control culture, glucose was fully consumed. For the glucose-D_7 – H_2O and glucose-D_7 - D_2O media some glucose remained after 96 h incubation at 25% and 16%, respectively.

This finding shows that glucose was not fully consumed using the glucose-D_7 substrate. The biomass yields for all samples is given in Table 3.1. The glucose - H_2O control sample had the highest yield (64 mg). The cells grown in glucose-D_7 - H_2O gave a 17% reduction in biomass yield while the glucose-D_7 - D_2O grown cells only had an 8% reduction compared to the control due to incomplete uptake of glucose. The effects of growth of microorganisms in D_2O have been long studied among the unicellular organisms [98][87][83]. For yeasts such as *S. cerevisiae* have revealed inhibited growth rates in 99% D_2O which has led to experimentation with deuterium resistant strains [99][100]. In another study on *Pichia pastoris* yeast, an elongated lag phase was observed with the introduction of a deuterated media resulting in the yeast cells taking more time to fully adjust and grow [88]. These studies support the observations in *Y. lipolytica* grown using labeled glucose in either H_2O or D_2O which would be hindering the metabolism of the cells. The lag phase introduced at the start sees a late growth of the cells with the experiments being performed for 96 h.

3.1.2 Lipid yield and composition

The lipid yields recorded after $CHCl_3$ extraction showed a change with the change in substrate as well (Table 3.1). The highest lipid yield was with the glucose control cultured sample (17.8%) followed by the glucose-D_7 - D_2O and the glucose-D_7 – H_2O grown cultures and were significantly different ($P<<0.05$, from student t-test, assuming equal variance). Lipid accumulation can depend upon several factors such as the growth media, growth time, and growth conditions [46]. Despite being an oleaginous microorganism, this relatively low lipid production in the purely glucose based media can be accounted towards the absence of N, where studies have shown that the lipid production was < 14-16% in N limited conditions [8], [10]. Also, the growth of *Y. lipolytica* using glucose as a sole C substrate has shown to produce very high amounts of citric acid and insignificant quantities of lipids [9]. Similar inferences were made in our study where the lipid production did not exceed 18% in any of the samples.

Studies for lipid profiles of various yeasts in the past has consistently shown C16 and C18 as the most synthesized lipids, usually produced through the *de novo* synthesis. In *S. cerevisiae,* one of the most widely studied yeast, palmitic (C16:0) and oleic (C18:1) acids make up for most of the lipid composition, unable to synthesize linoleic acid [101]. In other yeasts such as *P. pastoris* it has been shown that the amount of polyunsaturated fatty acids, mainly linoleic acid (C18:2) is much higher [88]. The FAME profiles for the biomass are shown in Figure 3.2 and results given in Table 3.2. The biomass, the extracts and the extracted biomass residues showed changes in their lipid profiles with changing substrates. The main fatty acids detected were palmitic, linoleic, oleic, and stearic (C18:0) acids dominating the overall yield. A variety of other fatty acids were also detected, ranging from

C14 to C24. Fatty acid composition was shown to be different whether the yeast was fed glucose in H_2O versus glucose-D_7 in H_2O and glucose-D_7 in D_2O (Table 3.2). *Y. lipolytica* is well known to produce unsaturated fatty acids, with oleic acid production being >50% closely followed by palmitic and linoleic acids [9], [102], [44]. The same has been observed in our case, where oleic acid production dominates at over 50% in the control sample.

The lipids from the biomass from deuterated substrates shows an overproduction of C18 fatty acids, 19% and 25% in glucose-D_7 – H_2O and glucose-D_7 - D_2O, respectively compared to the control sample as observed through the FAME analysis of the biomass and the lipid extracts. However, with the biomass grown in deuterated substrates, it was challenging to determine the difference between the deuterium incorporated C18:2 and C18:1 because of how closely they are in terms of their molecular weight and the characteristics of their mass spectra (Table 3.3). Nonetheless, the analysis of this peak shows a 66% and 51% reduction when grown in glucose-D_7 - H_2O and glucose-D_7 - D_2O respectively, in comparison to the C18:1 production in the control sample. This is a direct consequence of the substitution of deuterium into the substrate which slows down the introduction of double bonds [88], resulting in a reduction in the formation of unsaturated fatty acids. This phenomenon, the KIE, is responsible for the reduction in the rate of desaturation inside the cell with the rate of reduction depending upon the substitution of deuterium in a particular position [103], [104].

The peaks representing the FAME derivatives from the biomass grown deuterated substrates have shoulders corresponding to their non-deuterated counterparts (Figure 3.2), a result of the presence of both D and H in the deuterated incorporated substrates [105]. The deuterated FAME derivatives were shown to have a slightly shorter retention time than the non-labeled derivatives because of the difference in energy transfer between C–H and C–D

bonds as confirmed by the previous case studies [105]. The mass spectra for C16, C18, C18:2 and C18:1 was analyzed for their molecular ions (Table 3.3). The retention times and the molecular weights of these deuterated lipids vary with the change in the growth substrate, depending upon the amount of deuterium incorporated. The retention time corresponding to methyl palmitate in the control media sample has a retention time of 32.85 mins with (M^+ = m/z 270), compared to 32.72 mins (M^+ = m/z 279) for glucose-D_7 - H_2O media sample and 32.4 mins (M^+ = m/z 299) for glucose-D_7 - D_2O media sample (Figure 3.2). GCMS analysis was also performed on methyl D_{31}-palmitate standard (Appendix Figure 3) and has a M^+ = m/z 314. Similar trends were observed with other fatty acid methyl esters in the sample (Figure 3.3, 3.4, 3.5). This observation goes along with the change in retention times with the incorporation of deuterium by the cholesterol (cholesterol vs. D_7-cholesterol vs. D_{38}-cholesterol) as observed by Garcia et al. [95].

Table 3.1. Y. *lipolytica* biomass yield grown in three different media for 96 h (±s.d, n=3). For one way ANOVA with p>0.05, changes in the biomass yield (p=0.013, F(2, 6)=24.8) and the lipid extract (p=0.0001, F(2, 6)=73.6) with the change in substrate are significant.

Substrate	Biomass yield (mg)	$CHCl_3$ Lipid Extract (% of the biomass yield)
Glucose – H_2O	63.8±1.3	17.8±0.5
Glucose-D_7 – H_2O	53.5±2.7	13.5±0.4
Glucose-D_7 – D_2O	58.9±0.8	16.0±0.4

Table 3.2 Lipid extract yields from *Y. lipolytica* biomass and fatty acid profile of extract based on FAME analysis (±s. d, n=3). For ANOVA with p>0.05, the fatty acids C18:2 (p=0.03, F(1, 4)=9.8), C18:1 (p=0.0006, F(2, 6)=32.7) and d7-(C18:1/C18:2) (p=0.05, F(1, 4)=17.12) are significantly different with the change in substrate.

Compound		Amount (µg/mg)								
		Biomass			Extract			Residue		
		Glucose-H_2O	Glucose-D_7 -H_2O	Glucose-D_7 -D_2O	Glucose-H_2O	Glucose-D_7 -H_2O	Glucose-D_7 -D_2O	Glucose-H_2O	Glucose-D_7 -H_2O	Glucose-D_7 -D_2O
Myristic acid	C14	2.41±0.87	-	-	8.47±1.79	-	-	-	-	-
Pentadecanoic acid	C15	-	-	-	5.9±2.31	-	-	-	-	-
11-Hexadecenoic acid	C16:1	-	-	-	18.1±4.7	43.8±16.2	14.6±2.4	-	-	-
7-Hexadecenoic acid	C16:1	6.78±2.11	5.28±1.98	-	73.7±13.0	14.5±3.8	14.6±1.4	3.34±0.61	-	-
Palmitic acid*	C16	18.6±3.2	21.0±4.2	22.18±3.12	229±17	208±7	201±15	11.3±2.3	9.8±1.3	9.82±0.89
Margaric acid	C17	-	-	-	8.48±2.21	-	21.1±4.4	-	-	-
d7-(C18:1/C18:2)		-	45.5±4.7	68.5±6.3	-	344±19	491±35	-	21.6±3.3	22.4±5.6
Linoleic acid	C18:2	12.1±4.3	-	3.61±1.89	122±21	-	35.0±7.9	11.1±3.4	3.71±0.21	-
Oleic acid	C18:1	109±24	24.5±5.2	27.5±5.3	1015±58	108±23	148±12	27.3±3.3	3.94±0.78	-
Stearic acid*	C18	20.8±4.6	26±5.7	26.2±3.2	297±23	354±18	376±37	4.58±1.20	6.39±0.95	3.78±0.56
Arachidic acid	C20	0.44±0.08	0.62±0.23	0.43±0.06	10.5±2.2	16.7±4.6	8.28±3.43	-	-	-
Behenic acid	C22	0.61±0.17	0.95±0.20	0.92±0.19	63.6±7.9	35.9±4.6	22.7±5.6	4.33±0.87	2.80±1.03	-
Lignoceric acid	C24	0.87±0.98	1.01±0.32	1.09±0.57	26.4±2.5	21.8±4.9	22.2±2.3	-	-	-

* Note that the Gas Chromatogram of these methyl esters has a shoulder next to a peak indicating the production of both the lipid and its deuterated counterpart. The final amount in the table is a summation of both.

Table 3.3 The molecular ion (m/z) by electron impact mass spectrometry of fatty acid methyl esters from the *Y. lipolytica* grown in different media (glucose – H_2O, glucose-D_7 – H_2O, and glucose-D_7 – D_2O).

Lipid	Standard M^+ (m/z)	Glucose – H_2O	Glucose-D_7 - H_2O	Glucose-D_7 - D_2O
C16	270	270	279	299
C18:2/C18:1	294/296	294/296	306	327
C18	298	298	308	332

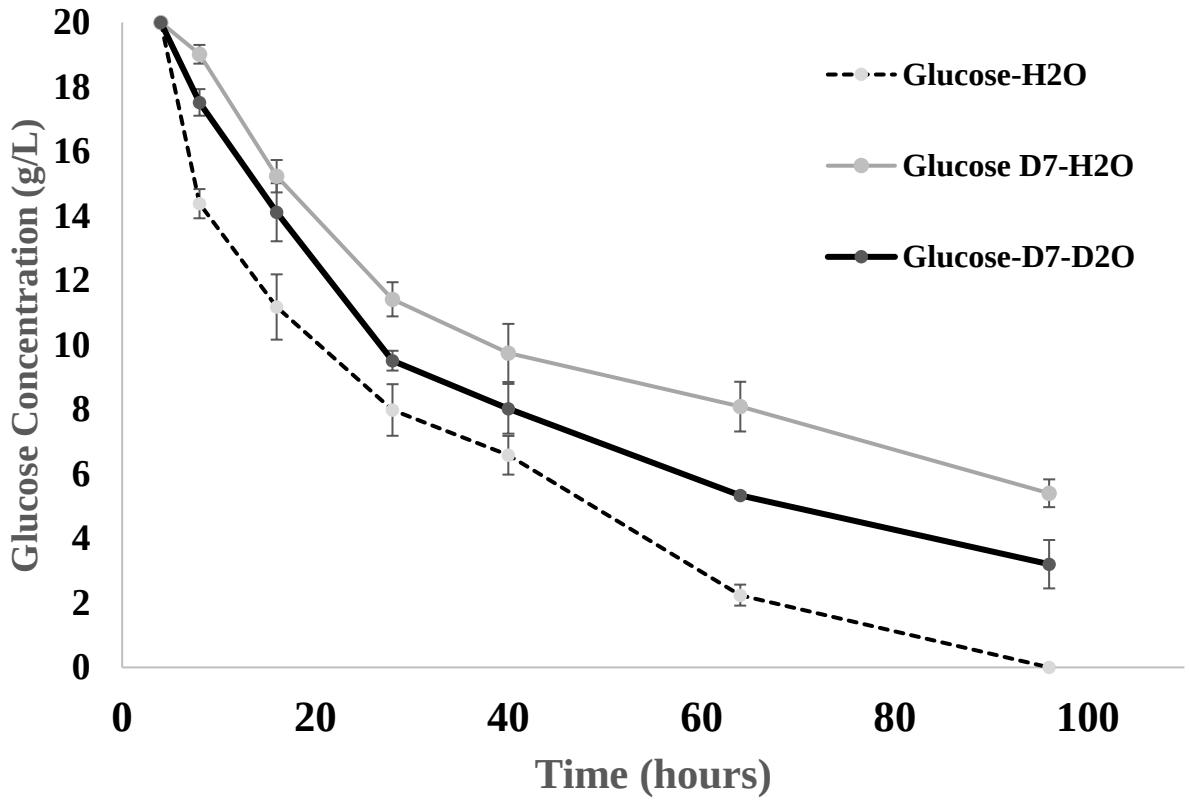

Figure 3.1: Consumption of glucose during incubation of *Y. lipolytica* grown in the following media: glucose – H_2O, glucose-D_7 – H_2O and glucose-D_7 - D_2O.

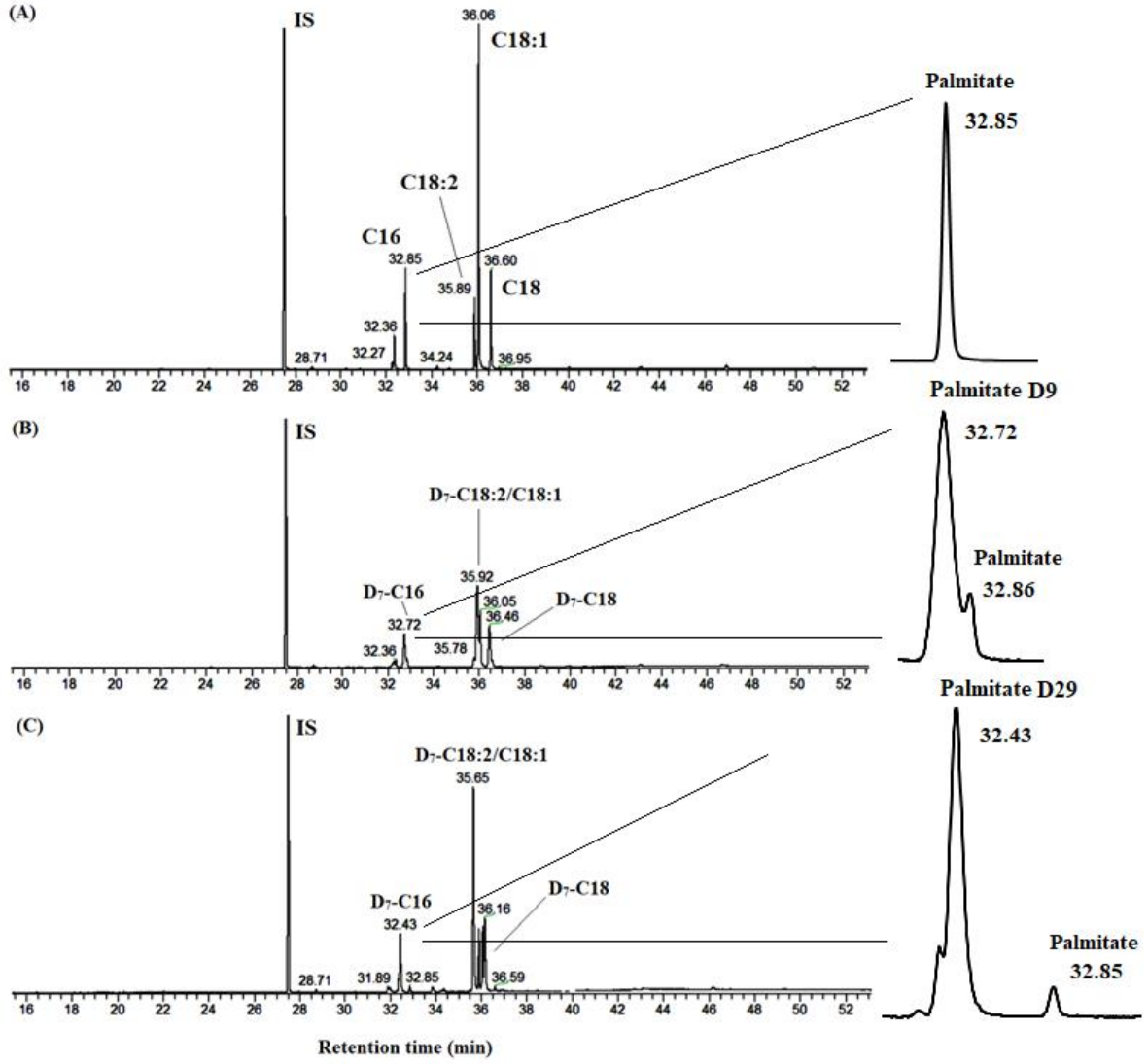

Figure 3.2: GCMS chromatogram representing fatty acid methyl esters (FAME) profiles from the *y. lipolytica* yeast grown in media (A) glucose – H_2O, (B) glucose-D_7 – H_2O, and (C) glucose-D_7 - D_2O. Note that deuterium incorporation into the fatty acids resulted in a change in retention times for the fatty acid methyl esters. Gas Chromatograph representing methyl palmitate and its retention times from the biomass grown in glucose – H_2O, glucose-D_7- H_2O, glucose-D_7 - D_2O have been expanded on the right side of the image. Note that with the incorporation of more deuterium from the substrate, the retention time of the lipid decreases as we move from (A) towards (C)

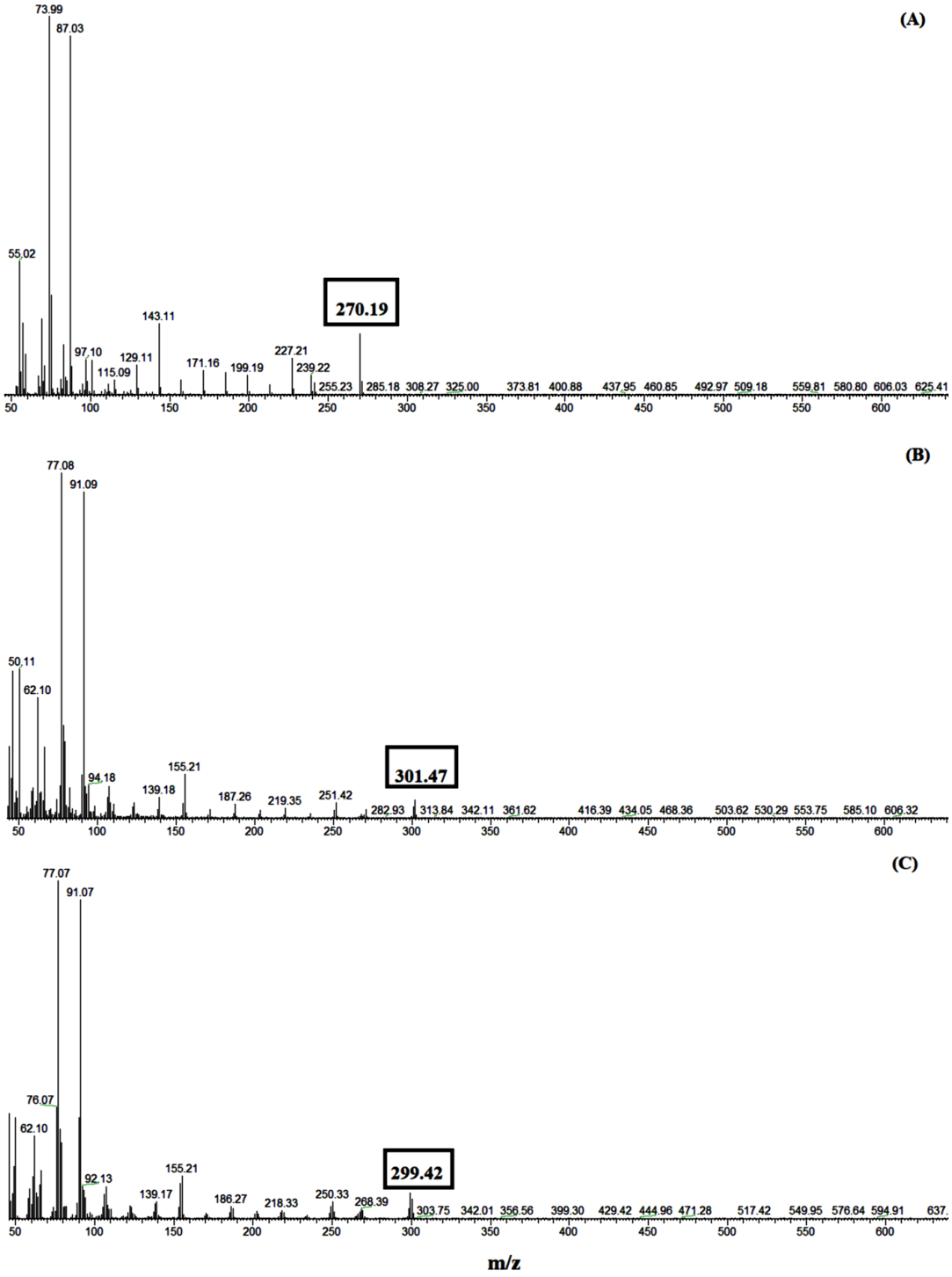

Figure 3.3: Mass spectra of fatty acid methyl ester derivatives of (A) palmitic acid (B) D_{31}-palmitic acid standard and (C) deuterium incorporated palmitic acid from lipid extracts of *Y. lipolytica* grown in glucose-D_7 - D_2O

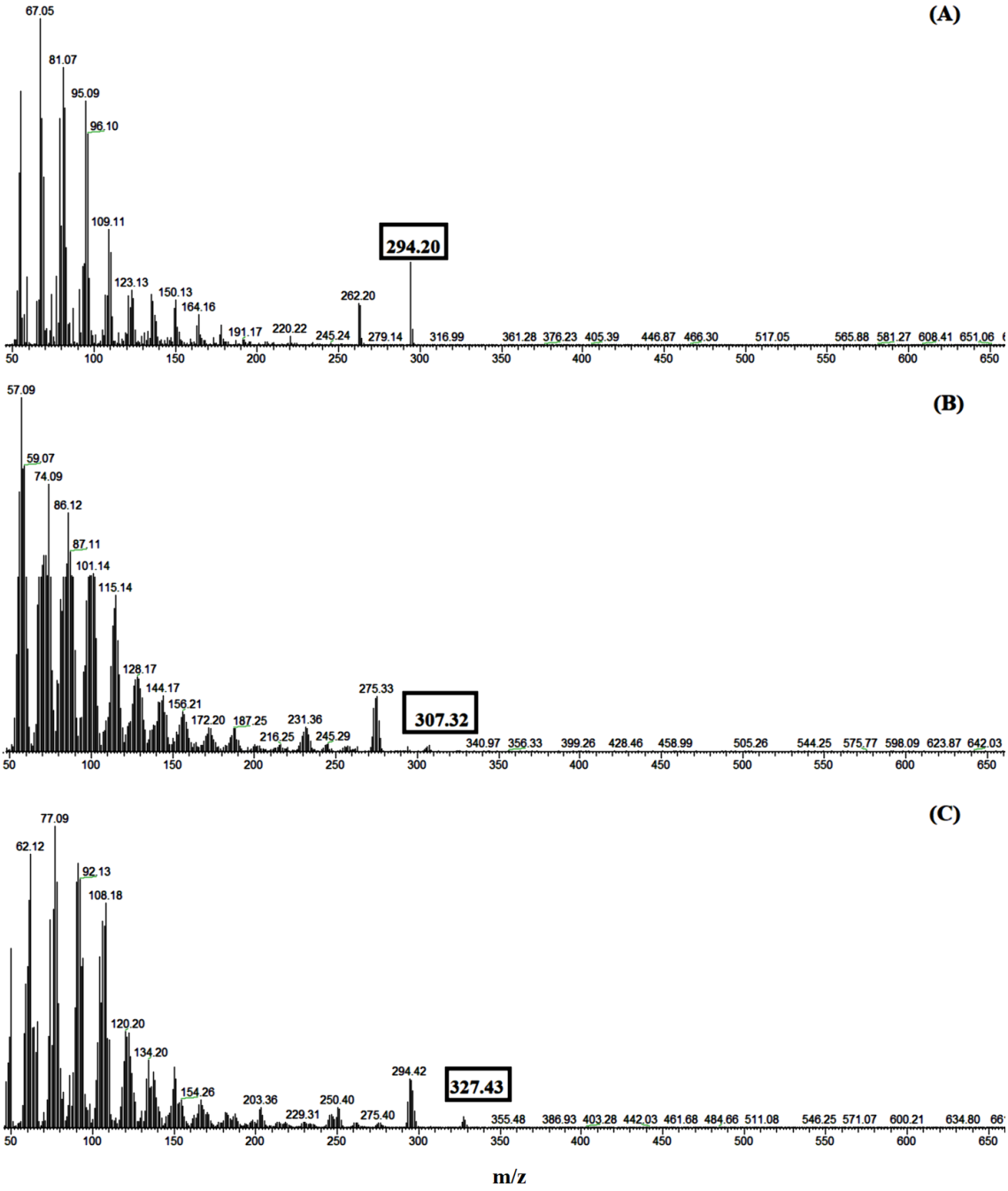

Figure 3.4: Mass spectra of fatty acid methyl ester derivatives of oleic, linoleic, and linolenic acids (/C18:1/C18:2) from the biomass grown using the following media (A) glucose-H_2O, (B) glucose-D_7 – H_2O, and (C) glucose-D_7 - D_2O.

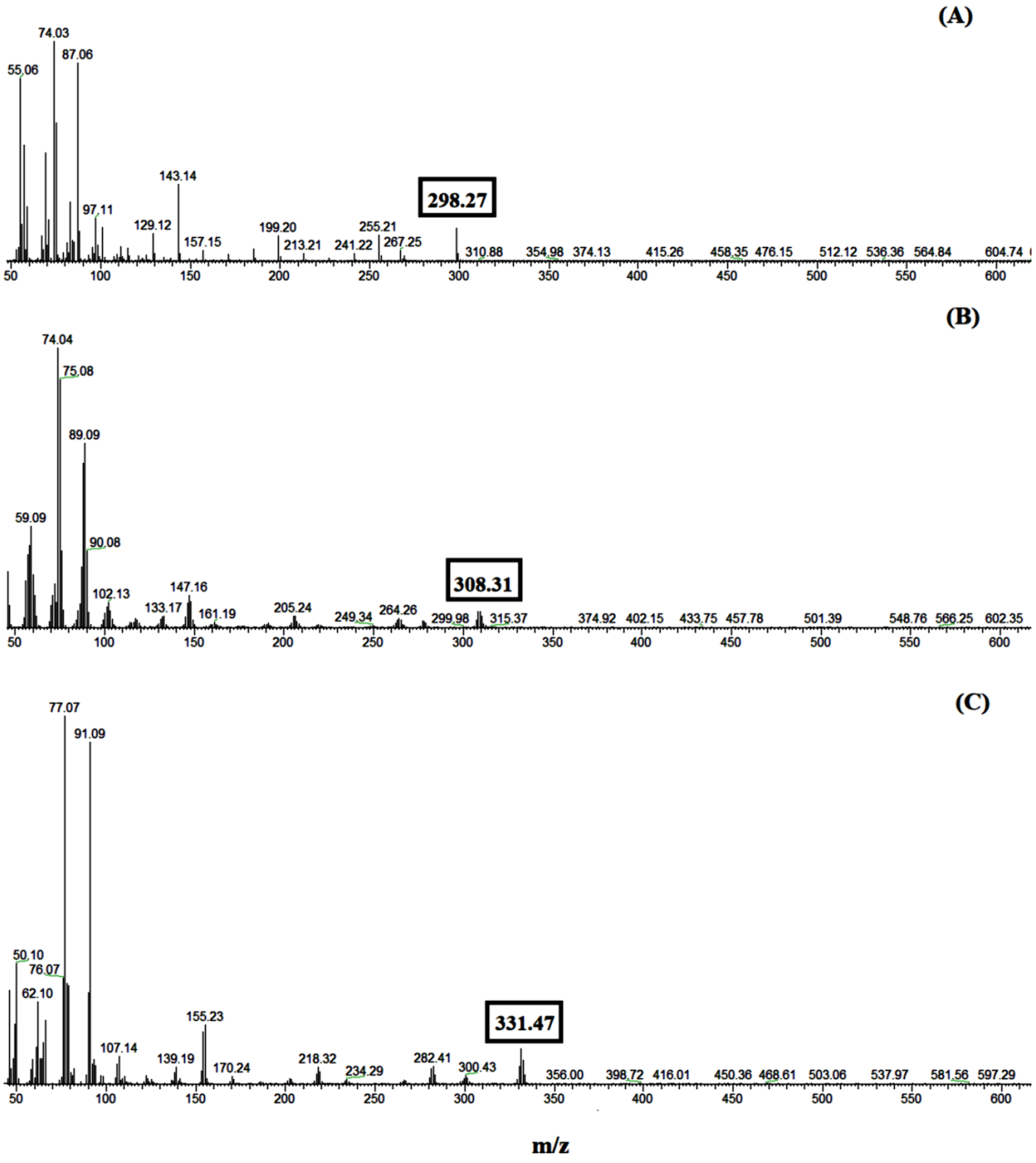

Figure 3.5: Mass spectra of fatty acid methyl ester derivatives of Stearic Acid from the biomass grown using the following media (A) glucose-H_2O, (B) glucose-D_7 – H_2O, (C) glucose-D^7 - D_2O.

3.2 Electrospray-mass spectrometry

Negative and positive ion ESI-MS was used to analyze intact TAGs in the lipid extracts for deuterium incorporation. The lipid extracts were analyzed for their molar mass (as molecular ions $[M+H]^+$ or $[M-H]^-$). Molar masses for the TAGs from the mass spectra were compared (Figure 3.6 and 3.7). TAGs $[M-H]^-$ions were observed for the lipid extracts from the biomass grown in glucose – H_2O at (*m/z* 806.37), (*m/z* 853.60) (*m/z* 881.64) and (*m/z* 907.62), while the positive $[M+H]^+$ ions at (*m/z* 808.37), (*m/z* 855.60) (*m/z* 883.64) and (*m/z* 909.62). These values were compared to a study based on the analysis of TAG from olive oil and the fatty acid compositions were discovered [106] (Table 3.4). *Y. lipolytica* has the capability to produce oleic, palmitic, and stearic acids in high quantities. Also based on the *m/z* values the TAGs at (*m/z* 806.37) and (*m/z* 907.62) were discovered as tripalmitin and triolein. Comparing the mass spectra of the control sample to the lipid extracts from deuterated substrates, a change in the mass was observed (Figure 3.6). For the lipid extracts from the *Y. lipolytica* yeast grown in glucose-D_7 – H_2O media the positive $[M+H]^+$ ions were detected at C48 (*m/z* 833.68), C50:1 (*m/z* 888.84) and C54:3 (*m/z* 943.94). And for the lipid extracts from the *Y. lipolytica* yeast grown in glucose-D_7 - D_2O the positive $[M+H]^+$ ions were detected at C48 (*m/z* 884.88), C50:1 (*m/z* 944.99) and C54:3 (*m/z* 1010.3). These elevated masses imply that the glucose-D_7 was not only incorporated into the TAGs but the presence of D_2O in the substrate substantially increases the net D incorporation into the yeast cells.

Table 3.4 ESI-MS analysis of TAGs found in *y. lipolytica* yeast grown in glucose-H_2O.

m/z $[M-H]^-$	***m/z*** $[M+H]^+$	**MW**	**TAG**	**Composition of the TAG**
806.66	808.63	807.67	C48	(16:0. 16:0, 16:0)
853.75	855.76	854.60	C50:1	(16:0, 16:0, 18:1)
877.79	879.79	878.79	C52:3	(16:0, 18:1, 18:2)
879.77	881.77	880.77	C52:2	(16:0, 18:1, 18:1)
903.70	905.70	904.70	C54:4	(18:1, 18:1, 18:2)
905.78	907.78	906.78	C54:3	(18:1, 18:1, 18:1)

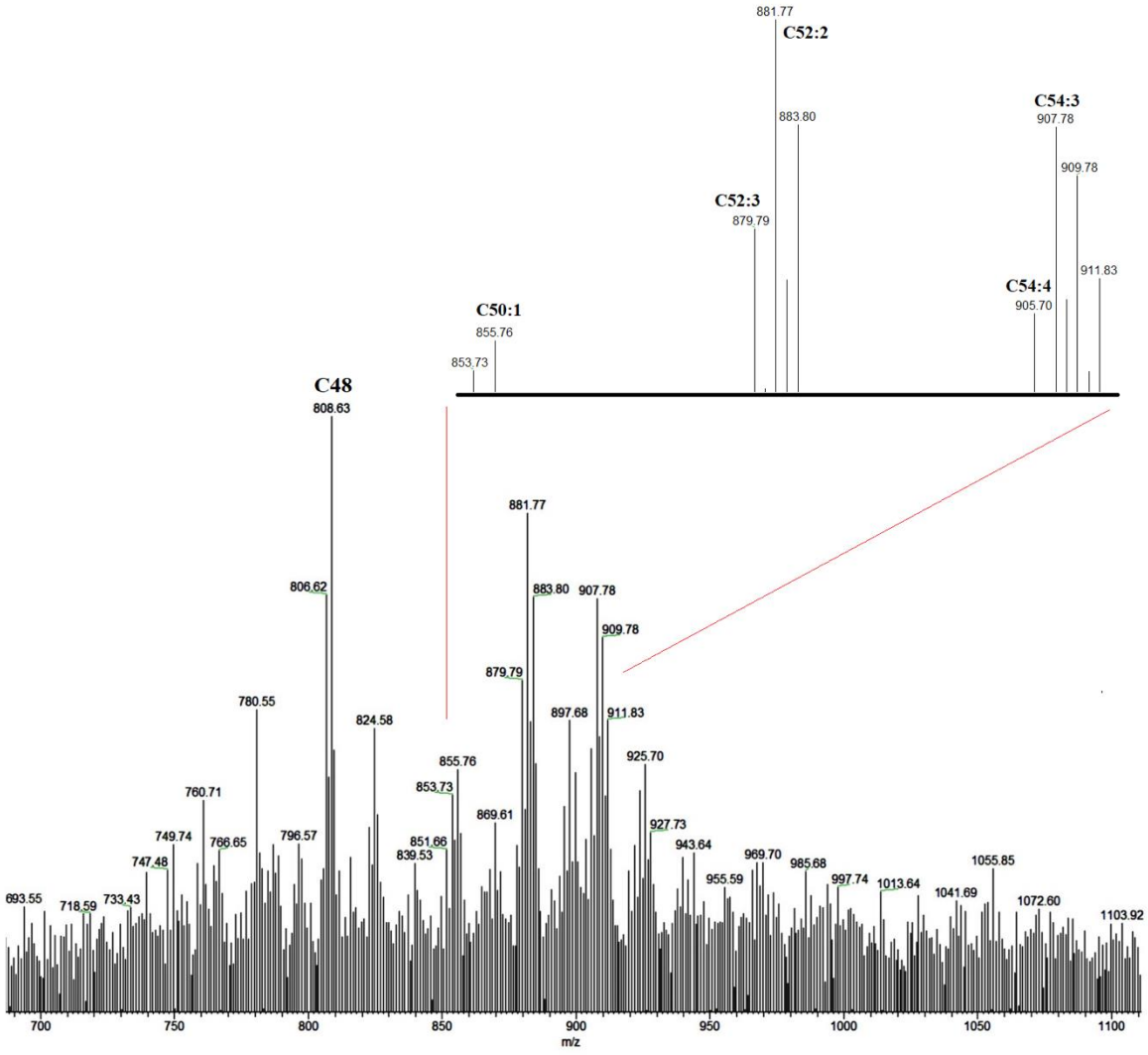

Figure 3.6 Positive ion electrospray mass spectra of lipid extracts from *Y. lipolytica* yeast grown in glucose – H_2O. The zoomed in portion highlights all the detected TAGs

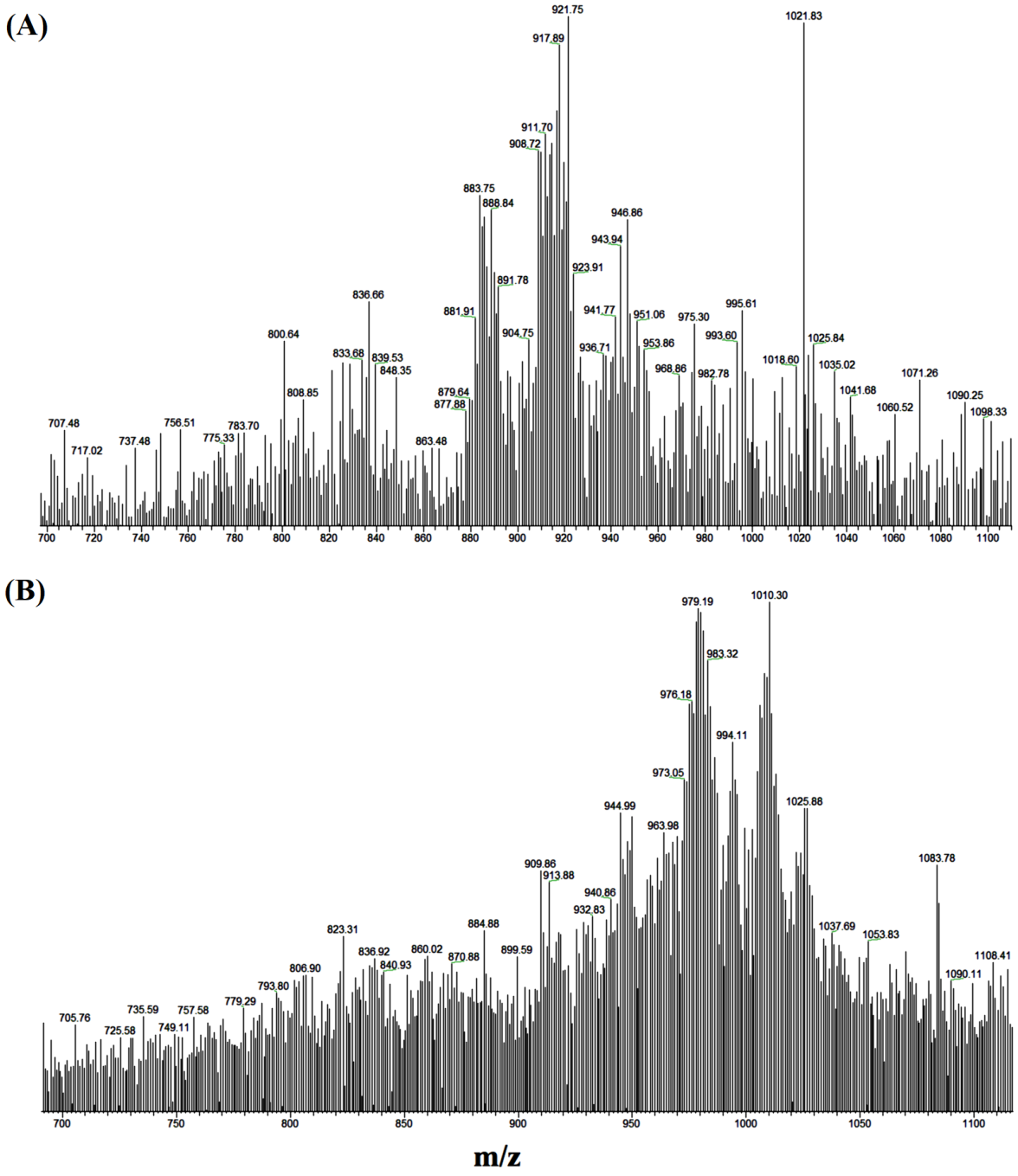

Figure 3.7. Positive ion electrospray mass spectra of lipid extracts from *Y. lipolytica* yeast grown in (A) glucose-D_7 – H_2O (B) glucose-D_7 - D_2O.

3.3 Sugar analysis

Sugar (as alditol acetates) and FAME analysis of the extracted biomass residue supports that glucose-D_7 was consumed in the presence of D_2O by the yeast. Table 3.5 shows the mass of monosaccharides present in the biomass residue from different obtained after lipid extraction. The results clearly depict that a large portion of glucose remains unused by the yeast when grown in glucose-D_7 substrate. The amount of unused glucose increases when the yeast is grown in glucose-D_7 - D_2O. Alongside glucose, mannose and galactose were also detected. Studies have shown the presence of galactose and mannose in the cell walls of *Y. lipolytica* in the form of β-glucan and mannan polysaccharides [107]. For the yeast *S. cerevisiae* the mechanical strength of the cell wall is mainly due to β1,3-glucan and in stationary phase cells, β1,3-glucan molecules has a degree of polymerization of 1500 glucose [108], [109]. A same observation has been made in a study for the formation of the cell walls of a fungi [110]. The observation implies that a portion of glucose from the substrate ends up in the formation of cell walls of *Y. lipolytica.*

GCMS analysis of the alditol acetates derivatives from the extracted biomass residues (grown on different media) hydrolysates in comparison to glucose, glucose-D_7, mannose and galactose standards show that deuterium was incorporated into the cell wall sugars (Figures 3.8 and 3.9). Glucitol acetate had a retention time of 16.67 min (*m/z* 360) and shifted to 16.57 min (*m/z* 367) for glucitol-D_7 acetate standard. This retention time shift was also observed in the FAME analysis. Glucose analysis of biomass residue grown on natural glucose in H_2O was identical to the glucitol acetate standard. The retention time for glucitol acetate grown on glucose-D_7 – H_2O (*m/z* 366) and glucose-D_7 – D_2O (*m/z* 366) media were the same as for glucitol-D7 standard (*m/z* 366) (Figures 3.8), as they show a slight shift for the deuterated

residues. In addition, the mass spectra for glucitol-D_7 standard and the deuterium incorporated glucose, mannose, and galactose in the biomass residue from glucose- D_7 and the residue from the glucose-D_7 - D_2O media were identical. This suggests that deuterium was retained in the sugars after biosynthesis of cell wall components.

Table 3.5. The weight and composition of sugars presents in the biomass residue after the extraction of lipids. Note that the retention time of glucose in deuterated incorporated biomass residues were less than that of biomass grown in control glucose media.

Saccharide	Amount per biomass yield (µg/mg)		
	Glucose – H_2O	Glucose-D_7 - H_2O	Glucose-D_7 - D_2O
Mannan	18.8	150	109
Galactan	2.2	16.4	8.6
Glucan	21.1	135	75.9

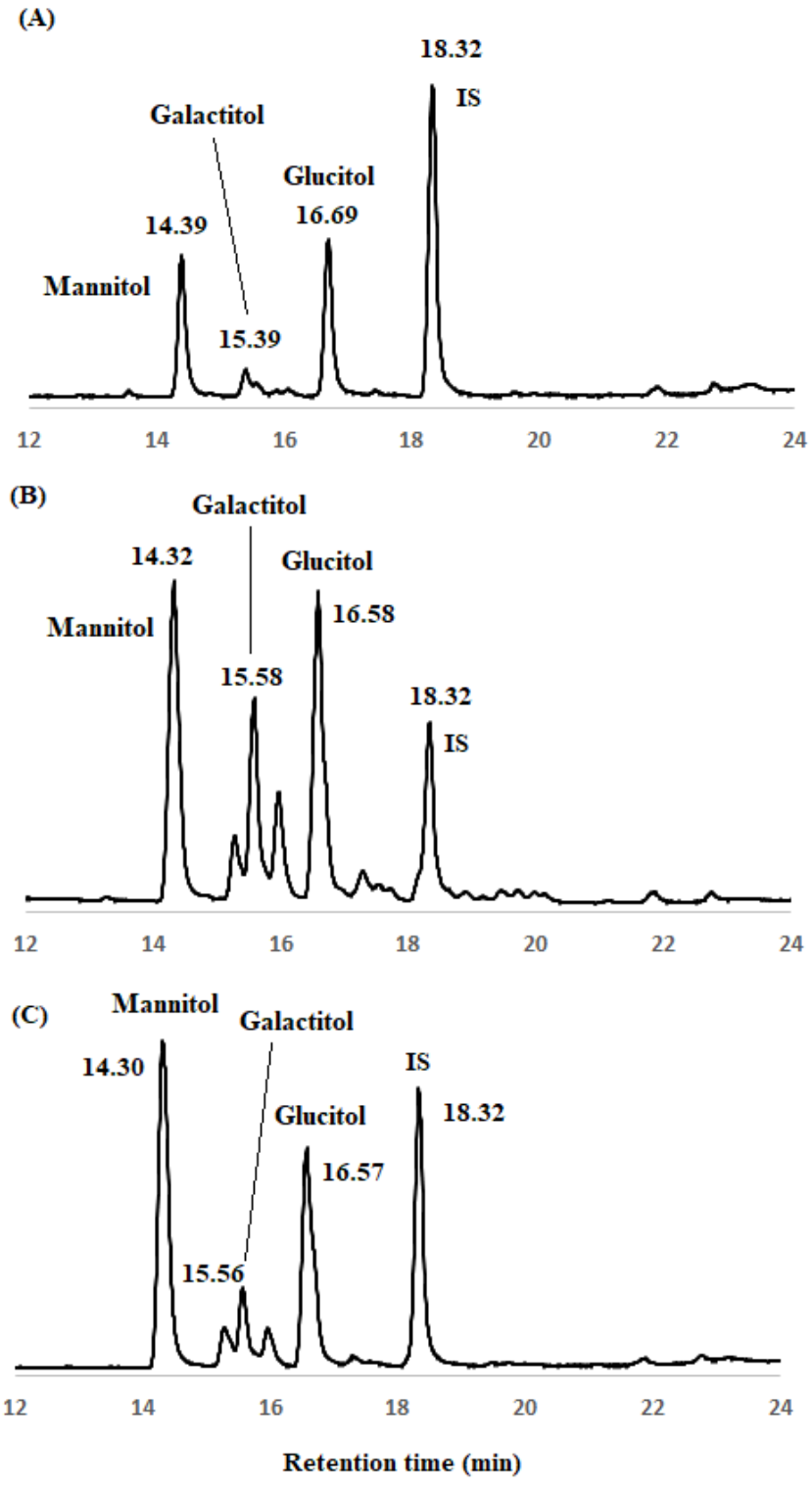

Figure 3.8: GCMS chromatogram representing carbohydrate (saccharide) profiles and retention times for the residues after lipid extraction from the *Y. lipolytica* yeast grown in media (A) glucose – H_2O, (B) glucose-D_7 – H_2O, and (C) glucose-D_7 - D_2O. Note that deuterium incorporation into the biomass resulted in a change in retention times for the saccharides

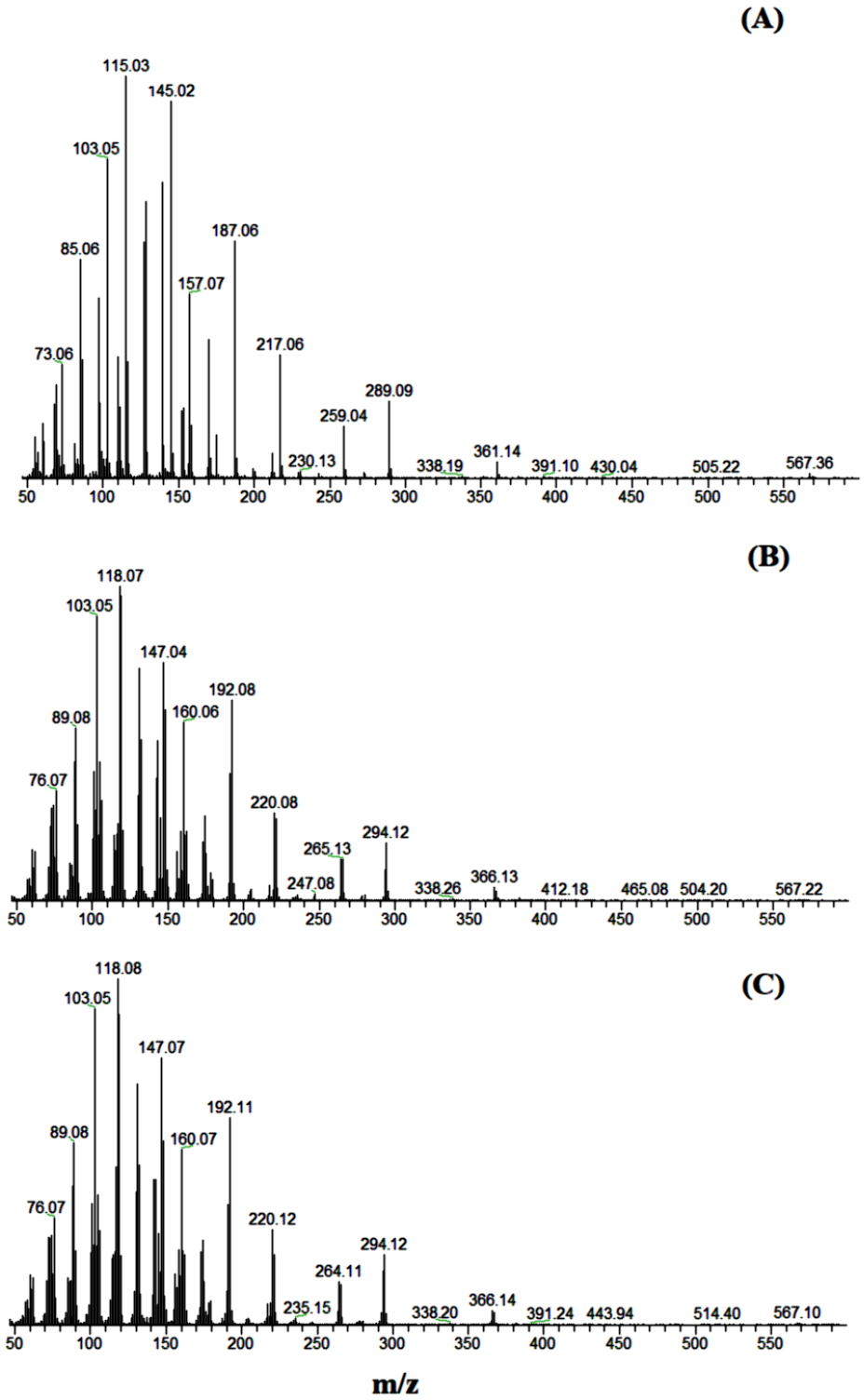

0

Figure 3.9: Mass spectra for the biomass residue after the lipid extraction from *y. lipolytica* yeast grown in (A) glucose – H_2O, (B) glucose-D_7 – H_2O, and (C) glucose-D_7 - D_2O highlighting the *m/z* values for Glucan.

3.4 Spectroscopy and band assignment

3.4.1 IR Spectroscopy

Infrared spectra in case of carbohydrates, lipids, proteins, and biomolecules generally represent two main regions of focus (i) 3100-2800 cm^{-1} for $-CH_3$ $-CH_2$ and (ii) 1800-1000 cm^{-1} for C-O-C, C-C and C-O, constituting of lipids, proteins, carbohydrates, polyphosphates, phospholipids and nucleic acids [58], [111]. With the strong dependence of vibrational spectroscopy on molecular mass, the frequency of deuterium incorporation is readily distinguishable from that of the hydrogen [112], [113]. As a rapid tool to examine changes in biomass chemistry associated with deuterium incorporation in the yeast, FTIR spectroscopy was performed on the dried biomass, lipid extracts and extracted biomass residue (Figure 3.10). Vibrational band assignments are given in Table 3.6. For the dried biomass samples a broad band at 3600-3100 cm^{-1} is attributed to O-H stretching vibrations in alcohols. C-H vibration bands associated with asymmetric stretching for CH_2 stretching were observed at 2922, 2919, and 2927 cm^{-1} for CH_3 [114] [56]. The C=O stretching band at 1740 cm^{-1} was assigned to esters associated with TAG [114], [115], [116], [117]. Bands at 1653 cm^{-1} and 1548 cm^{-1} were associated with Amide I and II bands of proteins [58]. C-O-C stretching band associated with polysaccharides were between 1252-1033 cm^{-1}.

The biomass produced using glucose-D_7 showed differences in their spectra compared to non-deuterated biomass. Due to the higher mass of D than H the frequency of C-D and O-D vibrations will be shifted to lower frequencies compared to C-H and O-H [118]. The presence of O-D stretching band is observed at 2470 cm^{-1} in the dried biomass grown on glucose-D_7 in D_2O and this has been observed in the literature [42], [49]–[51]. An asymmetric C-D_2

stretching band was seen at 2193 cm^{-1} (grown on glucose-D_7 in D_2O) while the C-D_2 symmetric stretching bands were observed at 2133 and 2114 cm^{-1} for biomass grown on glucose-D_7 and glucose-D_7 in D_2O, respectively [122].

FTIR spectra of extracted lipids (Figure 3.10) showed the presence of unsaturated fatty acids with =CH stretching bands at 3038 cm^{-1} (glucose control), 3007 cm^{-1} (glucose-D_7 in H_2O) and 3006 cm^{-1} (glucose-D_7 in D_2O). Deuterated labelled saturated lipids had CD_2 asymmetric and symmetric stretching bands at about 2193 and 2097 cm^{-1}, respectively. The CH_2 stretching band intensity decreased as deuterium was incorporated (CD_2) when grown in glucose-D_7 in D_2O media. The carbonyl ester band increased in intensity from the glucose control upon deuteration (Figure 3.10). For comparison, spectra for palmitic acid and D_{31}-palmitic acid clearly show the C-H bands at 2914 and 2847 cm^{-1} shifting to C-D bands at 2191 and 2088 cm^{-1} (Appendix Figure 1). The residual biomass after lipid extraction (Figure 3.9) showed a similar band to the yeast biomass. However, the intensity of the C-H stretching, C-D stretching and C=O stretching bands were of lower intensity in the residue compared to the original biomass for labelled and non-labelled samples due to lipid removal. The presence of CD_2 bands in the residue after lipid extraction in the glucose-D_7 in H_2O and glucose-D_7 in D_2O grown yeast was observed suggesting that deuterium was incorporated into non-lipid components, such as cell wall polysaccharides as confirmed by GCMS alditol acetate analysis.

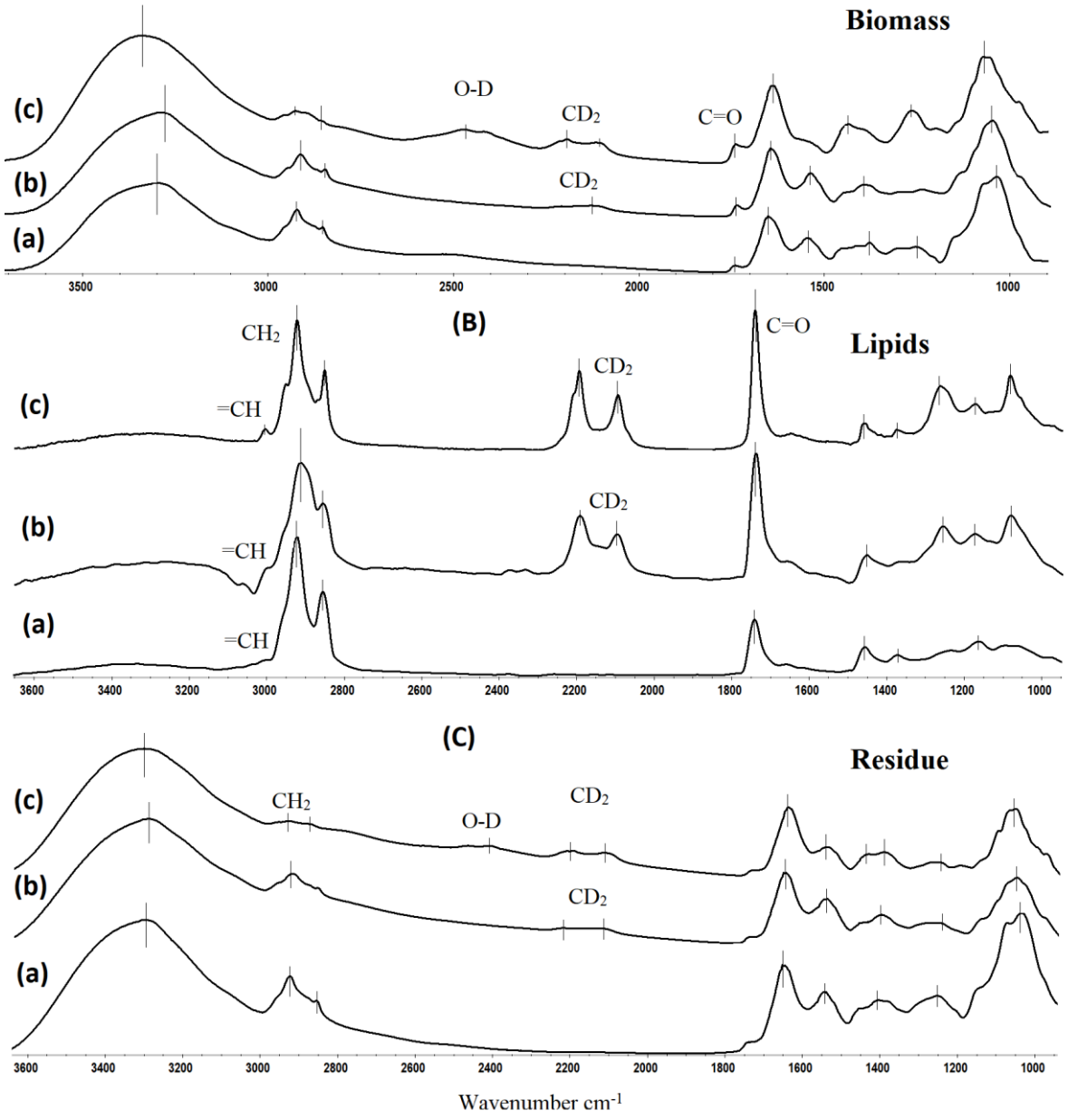

Figure 3.10: FTIR spectra of (A) *Y. lipolytica* biomass grown in (a) glucose in H_2O, (b) glucose-D_7 in H_2O, and (c) glucose-D_7 in D_2O, (B) lipids extracts from *Y. lipolytica* grown in (a) glucose in H_2O, (b) glucose-D_7 in H_2O, and (c) glucose-D_7 in D_2O, (C) extracted biomass residue from *Y. lipolytica* grown in (a) glucose in H_2O, (b) glucose-D_7 in H_2O, and (c) glucose-D_7 in D_2O.

Table 3.6: FTIR analysis results for the dried biomass, the lipid extract, and the extracted biomass residue from *Y. lipolytica* grown on different media. (**1* - Glucose-H_2O, 2* - Glucose-D_7-H_2O, 3* - Glucose-D_7-D_2O)**

	Biomass			**Extract**			**Extracted Residue**		
Band assignment	**1***	**2***	**3***	**1***	**2***	**3***	**1***	**2***	**3***
	Wavenumber (cm^{-1})								
CH stretch, unsaturated lipids	-	-	-	3362±3	3310±1	3266±4	-	-	-
O-H stretch, hydroxyl	3305±7	3303±3	3344±15	-	-	-	3294±4	3293±6	3306±7
C-H stretch (asymmetric), CH_2	2922±2	2919±6	2927±5	2923±8	2922±2	2923±4	2922±3	2919±11	2932±10
C-H stretch (symmetric), CH_2	2853±9	2852±12	2876±10	2852±2	2853±1	2853±3	2854±2	2853±6	2860±8
O-D stretch, D2O	-	-	2420±6	-	-	-	-	-	2412±2
C-D stretch (asymmetric) CD_2	-	-	2193±3	-	2193±7	2195±5	-	-	2196±4
C-D stretch (symmetric) CD_2	-	2133±11	2114±3	-	2097±12	2095±13	-	2117±7	2115±12
C=O stretch, ester of lipids	1739±3	1741±6	1738±7	1743±3	1741±3	1740±1	-	-	-
C=C stretch	1650±1	1650±3	1639±2				1650±2	1650±5	1640±3
C-H bending, CH_2	-	-	1434±6	1458±	1456±	1458±	1402±5	1397±3	1392±4
C-H stretch, CH_2 and CH_3,	1377±1	1395±5	-	1377±2	-	1377±1	-	-	-
C-O-C, C-C, C-O	1252±2	-	1262	-	1261	1275±1	1251±2	1247	1247
C-O-C, C-C, C-O	-	-	-	1162	1170±2	-	-	-	-
C-O-C, C-C, C-O	1033±3	1051±2	1055±1	-	1070±3	1083±5	1033±6	1047±2	1053±3

3.4.2 Raman spectroscopy

Raman spectroscopy was performed on the dried biomass, extracted lipids, and extracted biomass residue for all the cultured yeast samples (Figure 3.11). For non-labeled and labeled cultured *Y. lipolytica* biomass (Figure 3.11) major CH_3/CH_2 (C-H symmetric/asymmetric) stretching band was observed around 2930 cm^{-1}. The Raman spectra were of low resolution (~16 cm^{-1}) and sensitivity, compared to FTIR, and the CH_3 and CH_2, C-H stretching bands could not be resolved. In the biomass grown with glucose-D_7 in H_2O, the intensity of the C-H stretching band is reduced and a C-D stretching band (silent region) appears around 2222 cm^{-1} and 2147 cm^{-1}, corresponding to C-D_2 asymmetric and symmetric stretching, respectively. Similar C-D_2 stretches were observed at 2222 cm^{-1} and 2116 cm^{-1} corresponding to C-D_2 asymmetric and symmetric stretching respectively for the biomass grown with glucose-D_7 in D_2O. Furthermore, the intensity of the C-D band for the biomass grown in glucose-D_7 in D_2O was higher than in H_2O [123] [124]. The other major bands observed in the biomass spectra were the C=C alkyl stretching band at around 1655 cm^{-1} and C-C alkyl stretching band around 1120-1124 cm^{-1}. The presence of these bands and assignments were consistent with the Raman spectra of lipids in the literature [11], [12].

The extracted lipids were also examined by Raman spectroscopy (Figure 3.10). The non-labeled and deuterated incorporated lipid extracts showed the typical C-H stretching band at around 2930 cm^{-1}. The extracts from glucose-D_7 grown biomass were shown to have a C-D stretching band around 2183cm^{-1} and 2106 cm^{-1}, and for the extracts from glucose-D_7 in D_2O gown biomass at 2204cm^{-1} and 2107 cm^{-1} corresponding to C-D_2 asymmetric and symmetric stretching respectively, confirming the presence of deuterium incorporation in the lipids [67]. For comparison, spectra for palmitic acid and D_{31}-palmitic acid clearly show the C-H bands at

2800-2900 cm^{-1} shifting to C-D bands at 2195 cm^{-1} (asymmetric CD_2) and 2103 cm^{-1} (symmetric CD_2) stretches, respectively [42] (Appendix Figure 2). Similar results were pointed out by two studies on deuterated Raman probes where Alfonso-García et al. compares the differences in Raman shift of C-H bonding and C-D bonding using D_{38}-cholesterol [23] and Buchy et al. also reports similar spectra changes in the Raman silent region corresponding to C-D stretching of D_6-sequalenic acid [22]. To determine whether deuterium was still present in the biomass residue after extraction Raman spectroscopy was performed (Figure 3.11). The residual extracted biomass from the 3 samples had a characteristic C-H stretching band around 2928- 2963 cm^{-1}. The residual biomass from glucose-D_7 in H_2O and glucose-D_7 in D_2O grown cells both contained a C-D stretching band at 2149 cm^{-1}. This suggests that deuterium was either incorporated into other components (polysaccharides or protein) or in bound unextracted lipids. This supports the sugar analysis results which clearly show that deuterium was incorporated into the cell wall polysaccharides. The intensity of the Raman/FTIR peaks depends upon the concentration of the sample under observation, hence we see the variation in between the replicates through the standard deviation [126].

The difference in the intensity of C-H and C-D stretches via FTIR spectra was measured through peak fitting analysis, performed on the *Y. lipolytica* biomass using OriginPro 2019 (Origin LABS) (Appendix Figure 4) [119]. The ratio between the area under the C-D and C-H bands is 0.26 for the biomass grown in glucose-D_7 and 0.5 for the biomass grown in glucose-D_7+D_2O, implying that more deuterium was incorporated into the biomass when in D_2O versus H_2O. The same method was also used for Raman spectra where the ratio between the area under the C-D and C-H bands is 0.52 for the biomass grown in glucose-D_7 and 3.03 for the biomass grown in glucose-D_7+D_2O (Table 3.7).

Table 3.7: Area under the C-H and C-D stretches from the Raman/FTIR spectra of the biomass grown in glucose-D_7 + H_2O and glucose-D_7+D_2O (OriginPro 2019b).

Peak Ratio	Area (ratio)			
	FTIR		Raman	
	glucose-D_7	glucose-D_7 + D_2O	glucose-D_7	glucose-D_7 + D_2O
C-D/C-H(biomass)	0.26±0.05	0.5±0.1	0.52±0.2	3.03±1.09

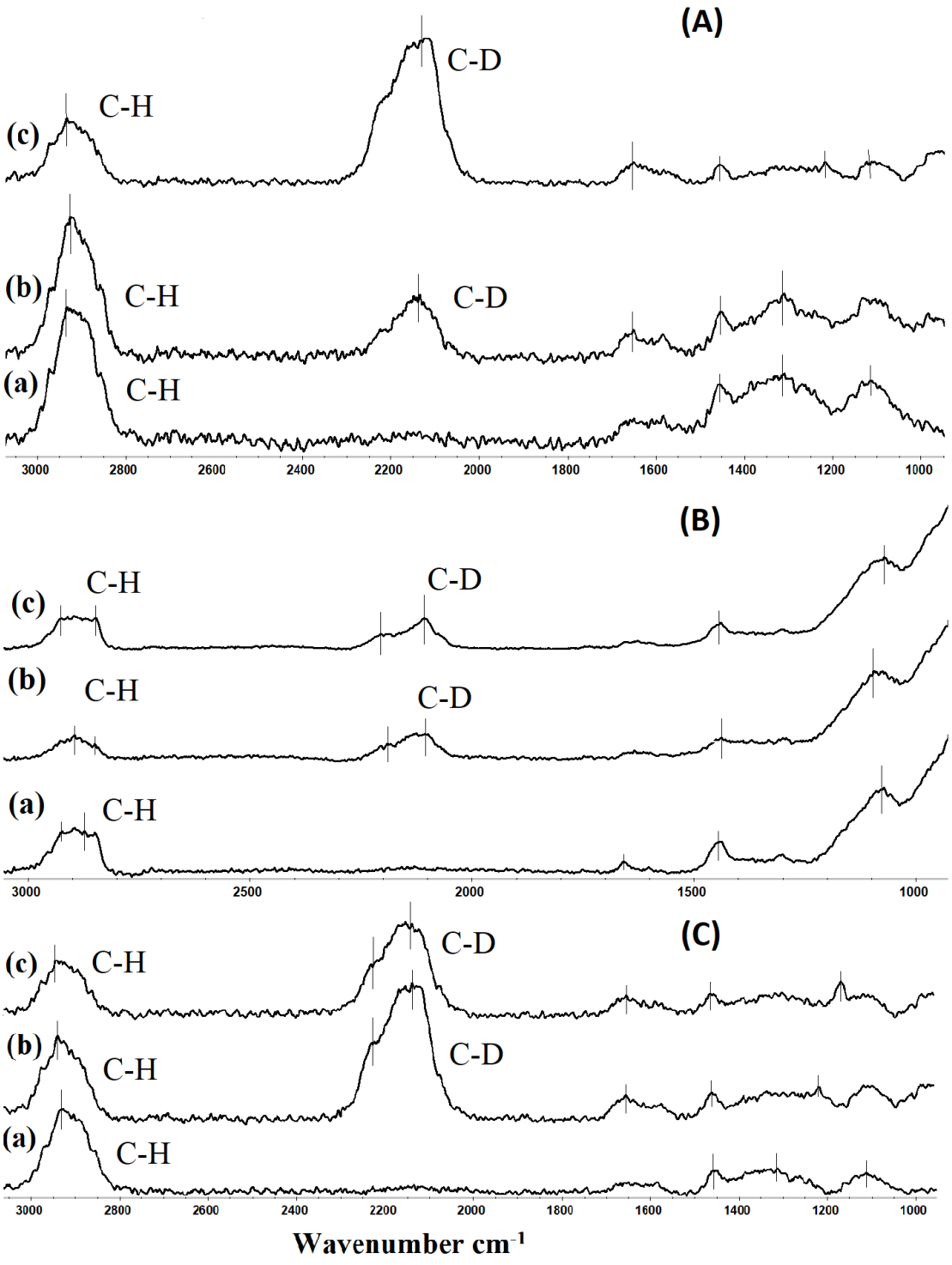

Figure 3.11: Raman spectra of (A) *Y. lipolytica* biomass grown in (a) glucose in H_2O, (b) glucose-D_7 in H_2O, and (c) glucose-D_7 in D_2O, (B) lipids extracts from *Y. lipolytica* grown in (a) glucose in H_2O, (b) glucose-D_7 in H_2O, and (c) glucose-D_7 in D_2O, and (C) extracted biomass residue from *Y. lipolytica* grown in (a) glucose in H_2O, (b) glucose-D_7 in H_2O, and (c) glucose-D_7 in D_2O.

3.5 Cell morphology

Yeast morphology was studied by optical microscopy. The yeast grown in the glucose – H_2O control sample were almost spherical in shape (Figure 3.12). While the yeasts grown in glucose-D_7– H_2O and glucose-D_7 – D_2O media were larger and elongated in shape with some irregularities. Image analysis was performed to determine the size of the cell populations. The distribution of the area data from the ImageJ software suggests non-normality (QQ plots and histograms of residuals, data not included), we compared the medians of the three groups. The median data points show a 0.009% increase in the area with the cells grown in glucose-D_7– H_2O and 0.05% increase with the cells grown in glucose-D_7 – D_2O compared to the control sample.

Taking into consideration the experimentation errors and the sample size under the study is relatively very small to the cell population. These factors imply that the change in the size of the cells seems too small to be termed as significant. Conclusively we can say that the effects of growing the yeast in a deuterated environment has negligible effects on the morphology of the cells.

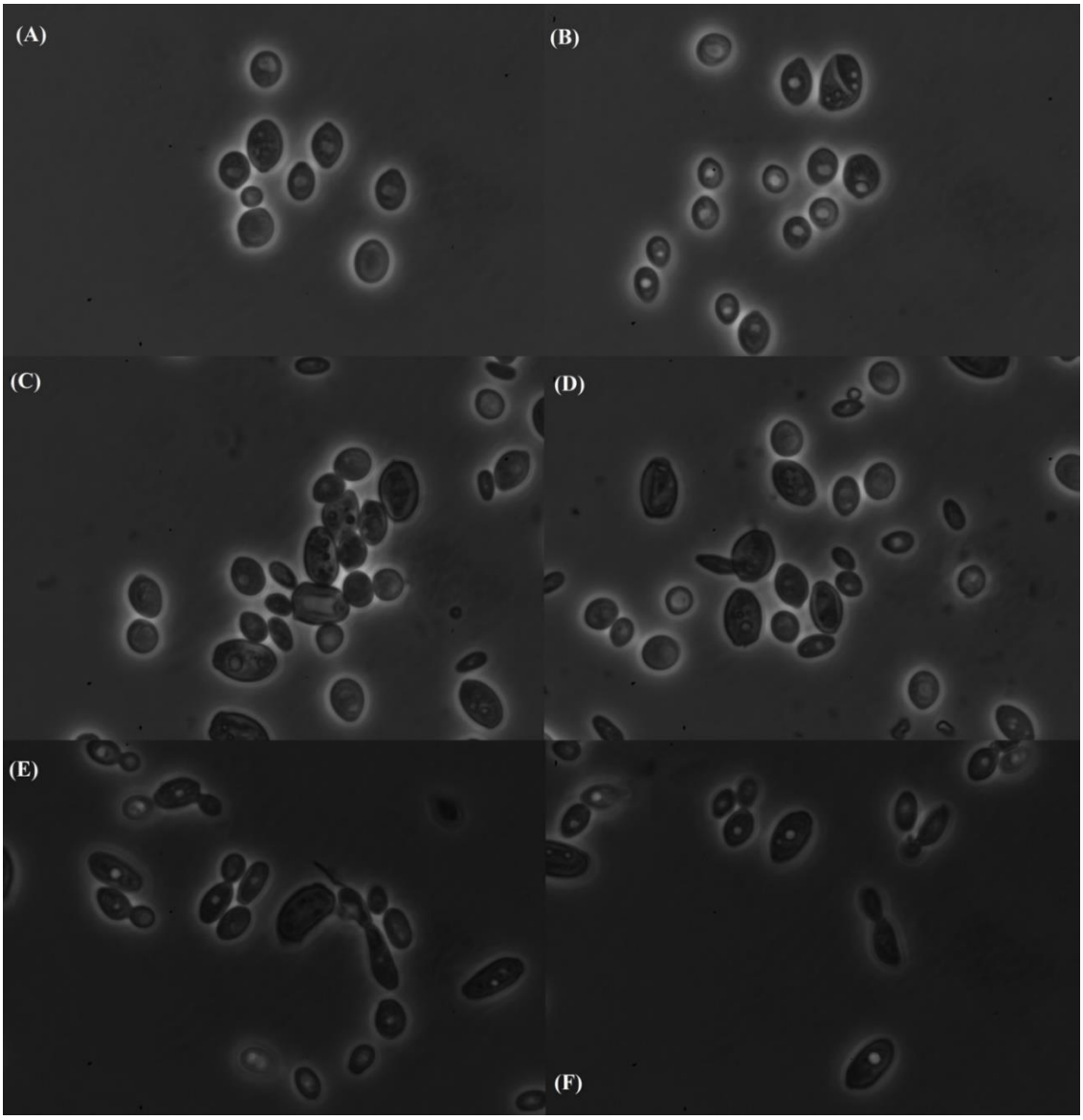

Figure 3.12: *Y. lipolytica* cells at 100x grown in (A) and (B) glucose in H_2O, (C) and (D) glucose-D_7 in H_2O, and (E) and (F) glucose-D_7 in D_2O.

Chapter 4: Conclusion

4.1 Conclusion

Y. lipolytica can be successfully grown in natural isotope abundant media under no N to produce lipids under optimum conditions (96 h) with an optical density >2.5. To study lipid formation in the yeast, cells were grown with no N in synthetic media with labelled glucose-D_7 in H_2O and glucose-D_7 in D_2O. The labeling was to see the deuterium incorporation into the lipids and other cellular components. The change in biomass and lipid yields were observed between non-labeled and D labeled media. Raman and FTIR spectroscopies on the biomass, the lipid extracts and the residue showed the incorporation of deuterium with a C-D band for the glucose-D_7 in H_2O grown cells and for cells grown on glucose-D_7 in D_2O media both in the Raman-silent region. The fatty acid profiles showed significant differences in lipid profiles between the 3 media types. Mass spectrometry was a useful tool to show the incorporation of deuterium. ESI-MS showed that deuterium was incorporated into the TAG by observing an increase in their molar mass when grown in glucose-D_7. The use of D_2O vs. H_2O also influenced (increased) the amount of deuterium incorporated into the lipids/fatty acids. The changes can be mitigated to a large extent via the use of D_2O along with glucose-D_7 resulting in a considerable increase in lipid yield, minimizing the deuterium-hydrogen exchange. The combination of FAME and carbohydrate analysis of the biomass residue after lipid extract shows a considerable amount of glucose-D_7 was not fully utilized in forming lipids but was also used in the biosynthesis of cell wall constituents by the presence of deuterium incorporation in the glucan, mannan and galactan polysaccharides.

4.2 Future Work

The overall goal of this project is to develop a multimodal imager for linking nutrient consumption and metabolic compartmentalization with the overall production performance of single living cells. The biomarkers produced through this experiment will be used as the precursors for the instrument, combining Light-sheet (LS) microscopy and Raman imaging on a single-cell scale. This will enable us to access the spatial and temporal metabolic dynamics in single cells, simultaneously enhancing the axial resolution and reducing the photodamage in comparison to the conventional fluorescence techniques.

References

[1] M. Höök, S. Davidsson, S. Johansson, and X. Tang, “Decline and depletion rates of oil production: a comprehensive investigation,” *Philos. Trans. R. Soc. Math. Phys. Eng. Sci.*, vol. 372, no. 2006, p. 20120448, Jan. 2014, doi: 10.1098/rsta.2012.0448.

[2] M. Guo, W. Song, and J. Buhain, “Bioenergy and biofuels: History, status, and perspective,” *Renew. Sustain. Energy Rev.*, vol. 42, pp. 712–725, Feb. 2015, doi: 10.1016/j.rser.2014.10.013.

[3] D. Kumar, B. Singh, and J. Korstad, “Utilization of lignocellulosic biomass by oleaginous yeast and bacteria for production of biodiesel and renewable diesel,” *Renew. Sustain. Energy Rev.*, vol. 73, pp. 654–671, Jun. 2017, doi: 10.1016/j.rser.2017.01.022.

[4] J. A. Gomez, K. Höffner, and P. I. Barton, “From sugars to biodiesel using microalgae and yeast,” *Green Chem.*, vol. 18, no. 2, Art. no. 2, 2016, doi: 10.1039/C5GC01843A.

[5] B. K. Shurtz, “Nutrient and Carbon-Dioxide Requirements for Large-Scale Microalgae Biofuel Production,” p. 80.

[6] M. Mirbagheri, I. Nahvi, G. Emtiazi, L. Mafakher, and F. Darvishi, “Taxonomic Characterization and Potential Biotechnological Applica- tions of Yarrowia lipolytica Isolated From Meat and Meat Products,” p. 6.

[7] M. Tai and G. Stephanopoulos, “Engineering the push and pull of lipid biosynthesis in oleaginous yeast Yarrowia lipolytica for biofuel production,” *Metab. Eng.*, vol. 15, pp. 1–9, Jan. 2013, doi: 10.1016/j.ymben.2012.08.007.

[8] S. Papanikolaou *et al.*, “Biosynthesis of lipids and organic acids by Yarrowia lipolytica strains cultivated on glucose,” *Eur. J. Lipid Sci. Technol.*, vol. 111, no. 12, pp. 1221–1232, Dec. 2009, doi: 10.1002/ejlt.200900055.

[9] S. Papanikolaou, M. Galiotou-Panayotou, I. Chevalot, M. Komaitis, I. Marc, and G. Aggelis, “Influence of Glucose and Saturated Free-Fatty Acid Mixtures on Citric Acid and Lipid Production by Yarrowia lipolytica,” *Curr. Microbiol.*, vol. 52, no. 2, pp. 134–142, Feb. 2006, doi: 10.1007/s00284-005-0223-7.

[10] S. Papanikolaou *et al.*, “Production of secondary metabolites through glycerol fermentation under carbon-excess conditions by the yeasts *Yarrowia lipolytica* and *Rhodosporidium toruloides*: Waste glycerol fermentation by yeasts,” *Eur. J. Lipid Sci. Technol.*, vol. 119, no. 9, p. 1600507, Sep. 2017, doi: 10.1002/ejlt.201600507.

[11] “Highly Efficient Biodiesel Conversion from Soybean Oil Using Liquid-Phase Plasma Discharge Technology.” https://doi.org/10.13031/trans.13534 (accessed Apr. 01, 2021).

[12] A. Beopoulos, J. Cescut, R. Haddouche, J.-L. Uribelarrea, C. Molina-Jouve, and J.-M. Nicaud, “Yarrowia lipolytica as a model for bio-oil production,” *Prog. Lipid Res.*, vol. 48, no. 6, Art. no. 6, Nov. 2009, doi: 10.1016/j.plipres.2009.08.005.

[13] “Hydrophobic substrate utilisation by the yeast Yarrowia lipolytica, and its potential applications | FEMS Yeast Research | Oxford Academic.” https://academic.oup.com/femsyr/article/5/6-7/527/528097 (accessed Jan. 19, 2021).

[14] W. J. Tipping, M. Lee, A. Serrels, V. G. Brunton, and A. N. Hulme, “Stimulated Raman scattering microscopy: an emerging tool for drug discovery,” *Chem. Soc. Rev.*, vol. 45, no. 8, pp. 2075–2089, Apr. 2016, doi: 10.1039/C5CS00693G.

[15] K.-C. Huang, J. Li, C. Zhang, Y. Tan, and J.-X. Cheng, “Multiplex Stimulated Raman Scattering Imaging Cytometry Reveals Lipid-Rich Protrusions in Cancer Cells under Stress Condition,” *iScience*, vol. 23, no. 3, Feb. 2020, doi: 10.1016/j.isci.2020.100953.

[16] D. Zhang, P. Wang, M. N. Slipchenko, and J.-X. Cheng, “Fast vibrational imaging of single cells and tissues by stimulated Raman scattering microscopy,” *Acc. Chem. Res.*, vol. 47, no. 8, pp. 2282–2290, Aug. 2014, doi: 10.1021/ar400331q.

[17] C. García-Timermans, R. Props, B. Zacchetti, M. Sakarika, F. Delvigne, and N. Boon, “Raman Spectroscopy-Based Measurements of Single-Cell Phenotypic Diversity in Microbial Populations,” *mSphere*, vol. 5, no. 5, Oct. 2020, doi: 10.1128/mSphere.00806-20.

[18] R. Mendelsoh, S. Sunder, and H. J. Bernstein, “DEUTERATED FATTY ACIDS AS RAMAN SPECTROSCOPIC PROBES OF MEMBRANE STRUCTURE,” p. 5.

[19] G. M. Walker, “Yeasts,” in *Encyclopedia of Microbiology (Third Edition)*, M. Schaechter, Ed. Oxford: Academic Press, 2009, pp. 478–491.

[20] J. B. Sutherland, C. Cornelison, and S. A. Crow, “CANDIDA | Yarrowia lipolytica (Candida lipolytica),” in *Encyclopedia of Food Microbiology*, Elsevier, 2014, pp. 374–378.

[21] P. Fontanille, V. Kumar, G. Christophe, R. Nouaille, and C. Larroche, “Bioconversion of volatile fatty acids into lipids by the oleaginous yeast Yarrowia lipolytica,” *Bioresour. Technol.*, vol. 114, pp. 443–449, Jun. 2012, doi: 10.1016/j.biortech.2012.02.091.

[22] M. A. Z. Coelho, P. F. F. Amaral, and I. Belo, “Yarrowia lipolytica: an industrial workhorse,” p. 16, 2010.

[23] A. L. Does and L. F. Bisson, “Comparison of glucose uptake kinetics in different yeasts,” *J. Bacteriol.*, vol. 171, no. 3, pp. 1303–1308, Mar. 1989, doi: 10.1128/jb.171.3.1303-1308.1989.

[24] F. Thevenieau, J.-M. Nicaud, and C. Gaillardin, “Applications of the Non-Conventional Yeast Yarrowia lipolytica,” in *Yeast Biotechnology: Diversity and Applications*, T. Satyanarayana and G. Kunze, Eds. Dordrecht: Springer Netherlands, 2009, pp. 589–613.

[25] C. L. Flores, C. Rodríguez, T. Petit, and C. Gancedo, “Carbohydrate and energy-yielding metabolism in non-conventional yeasts,” *FEMS Microbiol. Rev.*, vol. 24, no. 4, pp. 507–529, Oct. 2000, doi: 10.1111/j.1574-6976.2000.tb00553.x.

[26] G. Rodrigues and C. Pais, “The Influence of Acetic and Other Weak Carboxylic Acids on Growth and Cellular Death of the Yeast Yarrowia lipolytica,” p. 7.

[27] “Physiology and genetics of the dimorphic fungus Yarrowia lipolytica | FEMS Microbiology Reviews | Oxford Academic.” https://academic.oup.com/femsre/article/19/4/219/476967 (accessed Apr. 04, 2021).

[28] G. Barth and W. Künkel, “Alcohol dehydrogenase (ADH) in yeasts. II. NAD+-and NADP+-dependent alcohol dehydrogenases in Saccharomycopsis lipolytica,” *Z. Allg. Mikrobiol.*, vol. 19, no. 6, pp. 381–390, 1979, doi: 10.1002/jobm.3630190603.

[29] A. Dobrowolski, K. Drzymała, P. Mituła, and A. M. Mirończuk, “Production of tailor-made fatty acids from crude glycerol at low pH by Yarrowia lipolytica,” *Bioresour. Technol.*, vol. 314, p. 123746, Oct. 2020, doi: 10.1016/j.biortech.2020.123746.

[30] Z. Wang, J. Zhuge, H. Fang, and B. A. Prior, “Glycerol production by microbial fermentation: A review,” *Biotechnol. Adv.*, vol. 19, no. 3, pp. 201–223, Jun. 2001, doi: 10.1016/S0734-9750(01)00060-X.

[31] A. Braga, N. Gomes, and I. Belo, “Lipase Induction in Yarrowia lipolytica for Castor Oil Hydrolysis and Its Effect on γ-Decalactone Production,” *J. Am. Oil Chem. Soc.*, vol. 89, no. 6, pp. 1041–1047, 2012, doi: https://doi.org/10.1007/s11746-011-1987-5.

[32] M. Aguedo, M. H. Ly, I. Belo, J. A. Teixeira, J.-M. Belin, and Y. Waché, “The Use of Enzymes and Microorganisms for the Production of Aroma Compounds from Lipids,” p. 11, 2004.

[33] W. E. Levinson, C. P. Kurtzman, and T. M. Kuo, “Characterization of Yarrowia lipolytica and related species for citric acid production from glycerol,” *Enzyme Microb. Technol.*, vol. 41, no. 3, pp. 292–295, Aug. 2007, doi: 10.1016/j.enzmictec.2007.02.005.

[34] W. Rymowicz, A. Rywińska, B. Żarowska, and P. Juszczyk, “Citric acid production from raw glycerol by acetate mutants of Yarrowia lipolytica,” *Chem. Pap.*, vol. 60, no. 5, pp. 391–394, Oct. 2006, doi: 10.2478/s11696-006-0071-3.

[35] A. Crolla and K. J. Kennedy, “Optimization of citric acid production from Candida lipolytica Y-1095 using n-paraffin,” *J. Biotechnol.*, vol. 89, no. 1, pp. 27–40, Jul. 2001, doi: 10.1016/s0168-1656(01)00278-4.

[36] A. Te, S. Ia, S. Nv, and F. Tv, “Mathematical modeling of citric acid production by repeated batch culture,” *Enzyme Microb. Technol.*, vol. 26, no. 9–10, Jun. 2000, doi: 10.1016/s0141-0229(00)00178-2.

[37] S. K. Yalcin, M. T. Bozdemir, and Z. Y. Ozbas, “Citric acid production by yeasts: Fermentation conditions, process optimization and strain improvement,” p. 10, 2010.

[38] A. Fabiszewska, P. Misiukiewicz-Stępień, M. Paplińska-Goryca, B. Zieniuk, and E. Białecka-Florjańczyk, “An Insight into Storage Lipid Synthesis by Yarrowia lipolytica Yeast Relating to Lipid and Sugar Substrates Metabolism,” *Biomolecules*, vol. 9, no. 11, Nov. 2019, doi: 10.3390/biom9110685.

[39] S. D. Dyal and S. S. Narine, “Implications for the use of Mortierella fungi in the industrial production of essential fatty acids,” *Food Res. Int.*, vol. 38, no. 4, pp. 445–467, May 2005, doi: 10.1016/j.foodres.2004.11.002.

[40] M. Rossi, A. Amaretti, S. Raimondi, and A. Leonardi, “Getting Lipids for Biodiesel Production from Oleaginous Fungi,” in *Biodiesel - Feedstocks and Processing Technologies*, M. Stoytcheva, Ed. InTech, 2011.

[41] C. Ratledge and Z. Cohen, “Microbial and algal oils: Do they have a future for biodiesel or as commodity oils?,” *Lipid Technol.*, vol. 20, no. 7, pp. 155–160, 2008, doi: https://doi.org/10.1002/lite.200800044.

[42] S. Papanikolaou, I. Chevalot, M. Komaitis, G. Aggelis, and I. Marc, “Kinetic profile of the cellular lipid composition in an oleaginous Yarrowia lipolytica capable of producing a cocoa-butter substitute from industrial fats,” *Antonie Van Leeuwenhoek*, vol. 80, no. 3, pp. 215–224, Dec. 2001, doi: 10.1023/A:1013083211405.

[43] J. Rupcić, B. Blagović, and V. Marić, “Cell lipids of the Candida lipolytica yeast grown on methanol,” *J. Chromatogr. A*, vol. 755, no. 1, pp. 75–80, Nov. 1996, doi: 10.1016/s0021-9673(96)00579-1.

[44] K. Athenstaedt *et al.*, “Lipid particle composition of the yeastYarrowia lipolytica depends on the carbon source,” *PROTEOMICS*, vol. 6, no. 5, pp. 1450–1459, Mar. 2006, doi: 10.1002/pmic.200500339.

[45] A. M. Abdel-Mawgoud, K. A. Markham, C. M. Palmer, N. Liu, G. Stephanopoulos, and H. S. Alper, “Metabolic engineering in the host Yarrowia lipolytica,” *Metab. Eng.*, vol. 50, pp. 192–208, Nov. 2018, doi: 10.1016/j.ymben.2018.07.016.

[46] A. Beopoulos *et al.*, “Control of Lipid Accumulation in the Yeast Yarrowia lipolytica,” *Appl. Environ. Microbiol.*, vol. 74, no. 24, Art. no. 24, Dec. 2008, doi: 10.1128/AEM.01412-08.

[47] L.-T. Chuang, D.-C. Chen, J.-M. Nicaud, C. Madzak, Y.-H. Chen, and Y.-S. Huang, “Co-expression of heterologous desaturase genes in Yarrowia lipolytica,” *New Biotechnol.*, vol. 27, no. 4, pp. 277–282, Sep. 2010, doi: 10.1016/j.nbt.2010.02.006.

[48] K. Qiao *et al.*, “Engineering lipid overproduction in the oleaginous yeast Yarrowia lipolytica,” *Metab. Eng.*, vol. 29, pp. 56–65, May 2015, doi: 10.1016/j.ymben.2015.02.005.

[49] R. Ghogare, S. Chen, and X. Xiong, “Metabolic Engineering of Oleaginous Yeast Yarrowia lipolytica for Overproduction of Fatty Acids,” *Front. Microbiol.*, vol. 11, p. 1717, Jul. 2020, doi: 10.3389/fmicb.2020.01717.

[50] Z. Cui, C. Gao, J. Li, J. Hou, C. S. K. Lin, and Q. Qi, “Engineering of unconventional yeast Yarrowia lipolytica for efficient succinic acid production from glycerol at low pH,” *Metab. Eng.*, vol. 42, pp. 126–133, Jul. 2017, doi: 10.1016/j.ymben.2017.06.007.

[51] J. Sáez-Sáez, G. Wang, E. R. Marella, S. Sudarsan, M. Cernuda Pastor, and I. Borodina, “Engineering the oleaginous yeast Yarrowia lipolytica for high-level resveratrol production,” *Metab. Eng.*, vol. 62, pp. 51–61, Nov. 2020, doi: 10.1016/j.ymben.2020.08.009.

[52] N. R. Abu-Absi *et al.*, “Real time monitoring of multiple parameters in mammalian cell culture bioreactors using an in-line Raman spectroscopy probe,” *Biotechnol. Bioeng.*, vol. 108, no. 5, pp. 1215–1221, May 2011, doi: 10.1002/bit.23023.

[53] C.-C. Hsu *et al.*, “A single-cell Raman-based platform to identify developmental stages of human pluripotent stem cell-derived neurons,” *Proc. Natl. Acad. Sci.*, vol. 117, no. 31, pp. 18412–18423, Aug. 2020, doi: 10.1073/pnas.2001906117.

[54] R. Smith, K. L. Wright, and L. Ashton, “Raman spectroscopy: an evolving technique for live cell studies,” *Analyst*, vol. 141, no. 12, pp. 3590–3600, 2016, doi: 10.1039/C6AN00152A.

[55] P. Rösch, M. Harz, M. Schmitt, and J. Popp, “Raman spectroscopic identification of single yeast cells,” *J. Raman Spectrosc.*, vol. 36, no. 5, pp. 377–379, May 2005, doi: 10.1002/jrs.1312.

[56] E. Wiercigroch *et al.*, “Raman and infrared spectroscopy of carbohydrates: A review,” *Spectrochim. Acta. A. Mol. Biomol. Spectrosc.*, vol. 185, pp. 317–335, Oct. 2017, doi: 10.1016/j.saa.2017.05.045.

[57] M. Li, J. Xu, M. Romero-Gonzalez, S. A. Banwart, and W. E. Huang, “Single cell Raman spectroscopy for cell sorting and imaging,” *Curr. Opin. Biotechnol.*, vol. 23, no. 1, pp. 56–63, Feb. 2012, doi: 10.1016/j.copbio.2011.11.019.

[58] A. Rohman, A. Windarsih, E. Lukitaningsih, M. Rafi, K. Betania, and N. A. Fadzillah, “The use of FTIR and Raman spectroscopy in combination with chemometrics for analysis of biomolecules in biomedical fluids: A review,” *Biomed. Spectrosc. Imaging*, vol. 8, no. 3–4, pp. 55–71, Jan. 2019, doi: 10.3233/BSI-200189.

[59] K. Kochan *et al.*, “Pathological changes in the biochemical profile of the liver in atherosclerosis and diabetes assessed by Raman spectroscopy,” *Analyst*, vol. 138, no. 14, pp. 3885–3890, Jun. 2013, doi: 10.1039/C3AN00216K.

[60] K. Czamara, K. Majzner, M. Z. Pacia, K. Kochan, A. Kaczor, and M. Baranska, “Raman spectroscopy of lipids: a review: Raman spectroscopy of lipids,” *J. Raman Spectrosc.*, vol. 46, no. 1, pp. 4–20, Jan. 2015, doi: 10.1002/jrs.4607.

[61] C. Onogi and H. Hamaguchi, “Photobleaching of the ‘Raman Spectroscopic Signature of Life’ and Mitochondrial Activity in Rho− Budding Yeast Cells,” *J. Phys. Chem. B*, vol. 113, no. 31, pp. 10942–10945, Aug. 2009, doi: 10.1021/jp903478r.

[62] P.-T. Dong *et al.*, “Polarization-sensitive stimulated Raman scattering imaging resolves amphotericin B orientation in Candida membrane,” *Sci. Adv.*, vol. 7, no. 2, p. eabd5230, Jan. 2021, doi: 10.1126/sciadv.abd5230.

[63] C. W. Freudiger *et al.*, “Label-Free Biomedical Imaging with High Sensitivity by Stimulated Raman Scattering Microscopy,” *Science*, vol. 322, no. 5909, pp. 1857–1861, Dec. 2008, doi: 10.1126/science.1165758.

[64] W. Min, C. W. Freudiger, S. Lu, and X. S. Xie, “Coherent Nonlinear Optical Imaging: Beyond Fluorescence Microscopy,” *Annu. Rev. Phys. Chem.*, vol. 62, no. 1, pp. 507–530, 2011, doi: 10.1146/annurev.physchem.012809.103512.

[65] C.-Y. ChungBoik and E. O. Potma, “Biomolecular Imaging with Coherent Nonlinear Vibrational Microscopy,” *Annu. Rev. Phys. Chem.*, vol. 64, no. 1, pp. 77–99, 2013, doi: 10.1146/annurev-physchem-040412-110103.

[66] J.-X. Cheng and X. S. Xie, “Vibrational spectroscopic imaging of living systems: An emerging platform for biology and medicine,” *Science*, vol. 350, no. 6264, Nov. 2015, doi: 10.1126/science.aaa8870.

[67] L. Zhang *et al.*, “Spectral tracing of deuterium for imaging glucose metabolism,” *Nat. Biomed. Eng.*, vol. 3, no. 5, pp. 402–413, May 2019, doi: 10.1038/s41551-019-0393-4.

[68] “The Direct Analysis of Fermentation Products by Raman Spectroscopy - Thomas B. Shope, Thomas J. Vickers, Charles K. Mann, 1987.” https://journals.sagepub.com/doi/abs/10.1366/0003702874448373?journalCode=aspc (accessed Apr. 05, 2021).

[69] “Noninvasive, On-Line Monitoring of the Biotransformation by Yeast of Glucose to Ethanol Using Dispersive Raman Spectroscopy and Chemometrics - Adrian D. Shaw, Naheed Kaderbhai, Alun Jones, Andrew M. Woodward, Royston Goodacre, Jem J. Rowland, Douglas B. Kell, 1999.” https://journals.sagepub.com/doi/10.1366/0003702991945777 (accessed Apr. 05, 2021).

[70] S. Sivakesava, J. Irudayaraj, and A. Demirci, “Monitoring a bioprocess for ethanol production using FT-MIR and FT-Raman spectroscopy,” *J. Ind. Microbiol. Biotechnol.*, vol. 26, no. 4, pp. 185–190, Apr. 2001, doi: 10.1038/sj.jim.7000124.

[71] C. F. G. C. Geraldes, “Introduction to Infrared and Raman-Based Biomedical Molecular Imaging and Comparison with Other Modalities,” *Molecules*, vol. 25, no. 23, p. 5547, Nov. 2020, doi: 10.3390/molecules25235547.

[72] A. J. Berger, I. Itzkan, and M. S. Feld, “Feasibility of measuring blood glucose concentration by near-infrared Raman spectroscopy,” *Spectrochim. Acta. A. Mol. Biomol. Spectrosc.*, vol. 53A, no. 2, pp. 287–292, Feb. 1997, doi: 10.1016/s1386-1425(96)01779-9.

[73] A. M. K. Enejder *et al.*, “Raman spectroscopy for noninvasive glucose measurements,” *J. Biomed. Opt.*, vol. 10, no. 3, p. 031114, Jun. 2005, doi: 10.1117/1.1920212.

[74] K. L. Bechtel, W.-C. Shih, and M. S. Feld, “Intrinsic Raman spectroscopy for quantitative biological spectroscopy Part II: Experimental applications,” *Opt. Express*, vol. 16, no. 17, pp. 12737–12745, Aug. 2008, doi: 10.1364/OE.16.012737.

[75] E. Hirsch *et al.*, “Inline noninvasive Raman monitoring and feedback control of glucose concentration during ethanol fermentation,” p. 8.

[76] R. Schalk *et al.*, “Non-contact Raman spectroscopy for in-line monitoring of glucose and ethanol during yeast fermentations,” *Bioprocess Biosyst. Eng.*, vol. 40, no. 10, pp. 1519–1527, Oct. 2017, doi: 10.1007/s00449-017-1808-9.

[77] A. Němcová, D. Gonová, O. Samek, M. Sipiczki, E. Breierová, and I. Márová, “The Use of Raman Spectroscopy to Monitor Metabolic Changes in Stressed Metschnikowia sp. Yeasts,” *Microorganisms*, vol. 9, no. 2, p. 277, Jan. 2021, doi: 10.3390/microorganisms9020277.

[78] H. Wu, J. V. Volponi, A. E. Oliver, A. N. Parikh, B. A. Simmons, and S. Singh, “In vivo lipidomics using single-cell Raman spectroscopy,” *Proc. Natl. Acad. Sci.*, vol. 108, no. 9, pp. 3809–3814, Mar. 2011, doi: 10.1073/pnas.1009043108.

[79] H. C. Urey, F. G. Brickwedde, and G. M. Murphy, “A Hydrogen Isotope of Mass 2 and its Concentration,” *Phys. Rev.*, vol. 40, no. 1, pp. 1–15, Apr. 1932, doi: 10.1103/PhysRev.40.1.

[80] M. V. C. Cardoso, L. V. C. Carvalho, and E. Sabadini, “Solubility of carbohydrates in heavy water,” *Carbohydr. Res.*, vol. 353, pp. 57–61, May 2012, doi: 10.1016/j.carres.2012.03.005.

[81] P. Cioni and G. B. Strambini, “Effect of heavy water on protein flexibility,” *Biophys. J.*, vol. 82, no. 6, pp. 3246–3253, Jun. 2002, doi: 10.1016/S0006-3495(02)75666-X.

[82] T. Berg and D. H. Strand, “^{13}C labelled internal standards--a solution to minimize ion suppression effects in liquid chromatography-tandem mass spectrometry analyses of drugs in biological samples?,” *J. Chromatogr. A*, vol. 1218, no. 52, pp. 9366–9374, Dec. 2011, doi: 10.1016/j.chroma.2011.10.081.

[83] V. Kselíková, M. Vítová, and K. Bišová, “Deuterium and its impact on living organisms,” *Folia Microbiol. (Praha)*, vol. 64, no. 5, pp. 673–681, Sep. 2019, doi: 10.1007/s12223-019-00740-0.

[84] H. L. Crespi, S. M. Conard, R. A. Uphaus, and J. J. Katz, “Cultivation of microorganisms in heavy water,” *Ann. N. Y. Acad. Sci.*, vol. 84, pp. 648–666, Nov. 1960, doi: 10.1111/j.1749-6632.1960.tb39098.x.

[85] O. Mosin and I. Ignatov, “Phenomenon of Biological Adaptation to Heavy Water,” *J. Health Med. Nurs.*, vol. 6, no. 0, p. 73, 2014.

[86] W. Chorney, N. J. Scully, H. L. Crespi, and J. J. Katz, “The growth of algae in deuterium oxide,” *Biochim. Biophys. Acta*, vol. 37, pp. 280–287, Jan. 1960, doi: 10.1016/0006-3002(60)90235-3.

[87] O. W. Richards, “The Effect of Deuterium on the Growth of Yeast,” *J. Bacteriol.*, vol. 28, no. 3, pp. 289–294, Sep. 1934.

[88] A. de Ghellinck *et al.*, “Production and Analysis of Perdeuterated Lipids from Pichia pastoris Cells,” *PLoS ONE*, vol. 9, no. 4, p. e92999, Apr. 2014, doi: 10.1371/journal.pone.0092999.

[89] A. Naemat, H. M. Elsheikha, R. A. Boitor, and I. Notingher, “Tracing amino acid exchange during host-pathogen interaction by combined stable-isotope time-resolved Raman spectral imaging,” *Sci. Rep.*, vol. 6, p. 20811, Feb. 2016, doi: 10.1038/srep20811.

[90] K. S. Lee *et al.*, “An automated Raman-based platform for the sorting of live cells by functional properties,” *Nat. Microbiol.*, vol. 4, no. 6, Art. no. 6, Jun. 2019, doi: 10.1038/s41564-019-0394-9.

[91] J. Xu *et al.*, “Raman Deuterium Isotope Probing Reveals Microbial Metabolism at the Single-Cell Level,” *Anal. Chem.*, vol. 89, no. 24, pp. 13305–13312, Dec. 2017, doi: 10.1021/acs.analchem.7b03461.

[92] H.-J. van Manen, A. Lenferink, and C. Otto, “Noninvasive Imaging of Protein Metabolic Labeling in Single Human Cells Using Stable Isotopes and Raman Microscopy,” *Anal. Chem.*, vol. 80, no. 24, pp. 9576–9582, Dec. 2008, doi: 10.1021/ac801841y.

[93] D. Berry *et al.*, “Tracking heavy water (D2O) incorporation for identifying and sorting active microbial cells,” *Proc. Natl. Acad. Sci.*, vol. 112, no. 2, pp. E194–E203, Jan. 2015, doi: 10.1073/pnas.1420406112.

[94] D. J. Kushner, A. Baker, and T. G. Dunstall, “Pharmacological uses and perspectives of heavy water and deuterated compounds,” *Can. J. Physiol. Pharmacol.*, vol. 77, no. 2, pp. 79–88, Feb. 1999.

[95] A. Alfonso-García, S. G. Pfisterer, H. Riezman, E. Ikonen, and E. O. Potma, “D38-cholesterol as a Raman active probe for imaging intracellular cholesterol storage,” *J. Biomed. Opt.*, vol. 21, no. 6, p. 061003, Dec. 2015, doi: 10.1117/1.JBO.21.6.061003.

[96] E. Buchy *et al.*, “Synthesis of a deuterated probe for the confocal Raman microscopy imaging of squalenoyl nanomedicines,” *Beilstein J. Org. Chem.*, vol. 12, pp. 1127–1135, Jun. 2016, doi: 10.3762/bjoc.12.109.

[97] M. Chakraborty, A. G. McDonald, C. Nindo, and S. Chen, “An α-glucan isolated as a co-product of biofuel by hydrothermal liquefaction of Chlorella sorokiniana biomass,” *Algal Res.*, vol. 2, no. 3, pp. 230–236, Jul. 2013, doi: 10.1016/j.algal.2013.04.005.

[98] R. T. O’brien, “EFFECT OF D2O ON UPTAKE IN YEAST,” *Proc. Soc. Exp. Biol. Med. Soc. Exp. Biol. Med. N. Y. N*, vol. 117, pp. 555–558, Nov. 1964, doi: 10.3181/00379727-117-29636.

[99] A. Salvagno, “The biophysical effects of deuterium oxide on biomolecules and living cells through open notebook science.,” p. 131.

[100] K. Unno, T. Kishido, M. Morioka, S. Okada, and N. Oku, “Increased Expression of Hsp70 for Resistance to Deuterium Oxide in a Yeast Mutant Cell Line,” *Biol. Pharm. Bull.*, vol. 26, no. 6, pp. 799–802, 2003, doi: 10.1248/bpb.26.799.

[101] J. E. Stukey, V. M. McDonough, and C. E. Martin, “Isolation and characterization of OLE1, a gene affecting fatty acid desaturation from Saccharomyces cerevisiae,” *J. Biol. Chem.*, vol. 264, no. 28, pp. 16537–16544, Oct. 1989.

[102] P. Xu, K. Qiao, and G. Stephanopoulos, “Engineering oxidative stress defense pathways to build a robust lipid production platform in *Yarrowia lipolytica*: Engineering robust microbial oil cell factory,” *Biotechnol. Bioeng.*, vol. 114, no. 7, pp. 1521–1530, Jul. 2017, doi: 10.1002/bit.26285.

[103] P. H. Buist, “Fatty acid desaturases: selecting the dehydrogenation channel,” *Nat. Prod. Rep.*, vol. 21, no. 2, pp. 249–262, Apr. 2004, doi: 10.1039/b302094k.

[104] “Use of Deuterium Kinetic Isotope Effects To Probe the Cryptoregiochemistry of Δ9 Desaturation | Journal of the American Chemical Society.” https://pubs.acs.org/doi/abs/10.1021/ja953262n (accessed Mar. 25, 2021).

[105] M. Alzweiri, M. Khanfar, and Y. Al-Hiari, “Variations in GC–MS Response Between Analytes and Deuterated Analogs,” *Chromatographia*, vol. 78, no. 3–4, pp. 251–258, Feb. 2015, doi: 10.1007/s10337-014-2842-2.

[106] A. Kubo, T. Satoh, Y. Itoh, M. Hashimoto, J. Tamura, and R. B. Cody, “Structural Analysis of Triacylglycerols by Using a MALDI-TOF/TOF System with Monoisotopic Precursor Selection,” *J. Am. Soc. Mass Spectrom.*, vol. 24, no. 5, pp. 684–689, 2013, doi: 10.1007/s13361-012-0513-9.

[107] R. Vega and A. Dominguez, “Cell wall composition of the yeast and mycelial forms of Yarrowia lipolytica,” *Arch. Microbiol.*, 2004, doi: 10.1007/BF00414721.

[108] H. Weber, “A. H. Rose and J. S. Harrison (Editors), The Yeasts, Volume 2: Yeasts and the Environment (2nd Edition). XV + 309 S., 36 Abb., 28 Tab. London – Orlando – New York – San Diego – Austin – Boston – Sydney – Tokyo – Toronto 1987. Academic Press. $ 33.00. ISBN: 0-12-596412-9,” *J. Basic Microbiol.*, vol. 29, no. 7, pp. 436–436, 1989, doi: https://doi.org/10.1002/jobm.3620290711.

[109] M. A *et al.*, “The application of various protic acids in the extraction of (1-->3)-beta-D-glucan from Saccharomyces cerevisiae,” *Carbohydr. Res.*, vol. 299, no. 3, Apr. 1997, doi: 10.1016/s0008-6215(97)00004-9.

[110] J. Ruiz-Herrera and L. Ortiz-Castellanos, “Cell wall glucans of fungi. A review,” *Cell Surf.*, vol. 5, p. 100022, Dec. 2019, doi: 10.1016/j.tcsw.2019.100022.

[111] V. Shapaval *et al.*, “Biochemical profiling, prediction of total lipid content and fatty acid profile in oleaginous yeasts by FTIR spectroscopy,” *Biotechnol. Biofuels*, vol. 12, no. 1, p. 140, Jun. 2019, doi: 10.1186/s13068-019-1481-0.

[112] S. E. Lappi, B. Smith, and S. Franzen, “Infrared spectra of , and D2O in the liquid phase by single-pass attenuated total internal reflection spectroscopy,” *Spectrochim. Acta. A. Mol. Biomol. Spectrosc.*, vol. 60, no. 11, pp. 2611–2619, Sep. 2004, doi: 10.1016/j.saa.2003.12.042.

[113] J. E. Bertie, M. K. Ahmed, and H. H. Eysel, “Infrared intensities of liquids. 5. Optical and dielectric constants, integrated intensities, and dipole moment derivatives of water and water-d2 at 22.degree.C,” *J. Phys. Chem.*, vol. 93, no. 6, pp. 2210–2218, Mar. 1989, doi: 10.1021/j100343a008.

[114] K. Forfang, B. Zimmermann, G. Kosa, A. Kohler, and V. Shapaval, “FTIR Spectroscopy for Evaluation and Monitoring of Lipid Extraction Efficiency for Oleaginous Fungi,” *PLOS ONE*, vol. 12, no. 1, p. e0170611, Jan. 2017, doi: 10.1371/journal.pone.0170611.

[115] W. Mihoubi, E. Sahli, A. Gargouri, and C. Amiel, “FTIR spectroscopy of whole cells for the monitoring of yeast apoptosis mediated by p53 over-expression and its suppression by Nigella sativa extracts,” *PLOS ONE*, vol. 12, no. 7, p. e0180680, Jul. 2017, doi: 10.1371/journal.pone.0180680.

[116] C. Yu and J. Irudayaraj, “Spectroscopic characterization of microorganisms by Fourier transform infrared microspectroscopy,” *Biopolymers*, vol. 77, no. 6, pp. 368–377, Apr. 2005, doi: 10.1002/bip.20247.

[117] M. Taha, M. Hassan, S. Essa, and Y. Tartor, “Use of Fourier transform infrared spectroscopy (FTIR) spectroscopy for rapid and accurate identification of Yeasts isolated from human and animals,” *Int. J. Vet. Sci. Med.*, vol. 1, no. 1, pp. 15–20, Jun. 2013, doi: 10.1016/j.ijvsm.2013.03.001.

[118] D. M. Hudgins, C. W. Bauschlicher, Jr., and S. A. Sandford, “The Impact of Deuteration on the Infrared Spectra of Interstellar Polycyclic Aromatic Hydrocarbons,” *Astrophys. J.*, vol. 614, no. 2, pp. 770–780, Oct. 2004, doi: 10.1086/423930.

[119] K. Park, Y. Kim, and K. J. Lee, “Analysis of deuterated water contents using FTIR bending motion,” *J. Radioanal. Nucl. Chem.*, vol. 322, no. 2, pp. 487–493, Nov. 2019, doi: 10.1007/s10967-019-06734-z.

[120] J.-J. Max and C. Chapados, “Isotope effects in liquid water by infrared spectroscopy,” *J. Chem. Phys.*, vol. 116, no. 11, pp. 4626–4642, Mar. 2002, doi: 10.1063/1.1448286.

[121] I. Litvak, Y. Anker, and H. Cohen, “On-line *in situ* determination of deuterium content in water *via* FTIR spectroscopy,” *RSC Adv.*, vol. 8, no. 50, pp. 28472–28479, 2018, doi: 10.1039/C8RA03312A.

[122] E. Tyrode and J. Hedberg, “A Comparative Study of the CD and CH Stretching Spectral Regions of Typical Surfactants Systems Using VSFS: Orientation Analysis of the Terminal CH_3 and CD_3 Groups,” *J. Phys. Chem. C*, vol. 116, no. 1, pp. 1080–1091, Jan. 2012, doi: 10.1021/jp210013g.

[123] S. Sunder, R. Mendelsohn, and H. J. Bernstein, “Raman studies of the C-H and C-D stretching regions in stearic acid and some specifically deuterated derivatives,” *Chem. Phys. Lipids*, vol. 17, no. 4, pp. 456–465, Nov. 1976, doi: 10.1016/0009-3084(76)90047-5.

[124] G. Di Lonardo, L. Fusina, E. Canè, F. Tamassia, R. Z. Martínez, and D. Bermejo, “High resolution infrared and Raman spectra of $^{13}C\,^{12}CD_2$: The CD stretching fundamentals and associated combination and hot bands,” *J. Chem. Phys.*, vol. 143, no. 9, p. 094302, Sep. 2015, doi: 10.1063/1.4929723.

[125] C. Petrokilidou *et al.*, “The lipid profile of three Malassezia species assessed by Raman spectroscopy and discriminant analysis,” *Mol. Cell. Probes*, vol. 46, p. 101416, Aug. 2019, doi: 10.1016/j.mcp.2019.06.006.

[126] Y. Han, L. Han, Y. Yao, Y. Li, and X. Liu, “Key factors in FTIR spectroscopic analysis of DNA: the sampling technique, pretreatment temperature and sample concentration,” *Anal. Methods*, vol. 10, no. 21, pp. 2436–2443, May 2018, doi: 10.1039/C8AY00386F.

Appendix

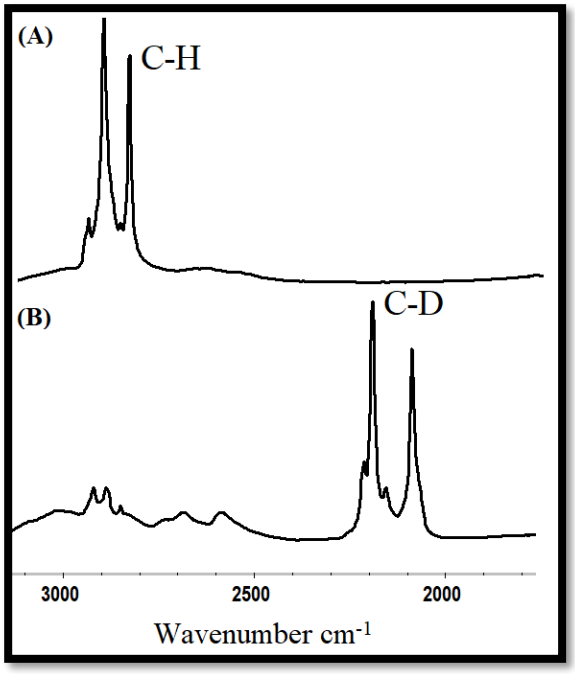

Figure 1: FTIR spectra of (A) palmitic acid and (B) D_{31}-palmitic acid

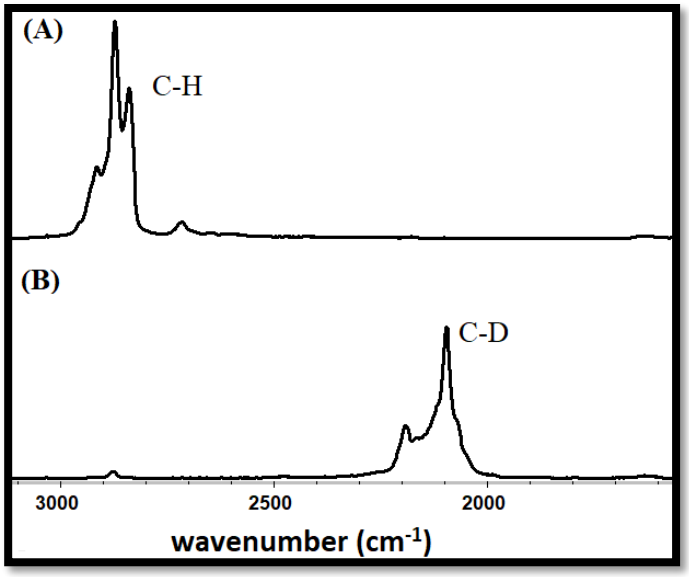

Figure 2: Raman spectra of (A) palmitic acid and (B) D_{31}-palmitic acid

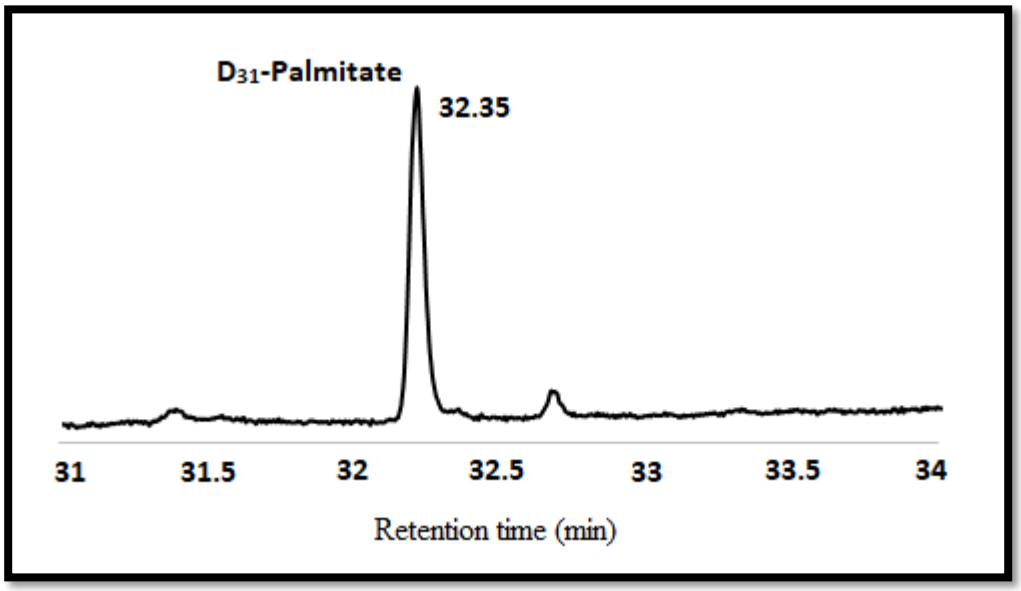

Figure 3: GCMS Chromatogram of the D_{31}-Palmitic Acid standard

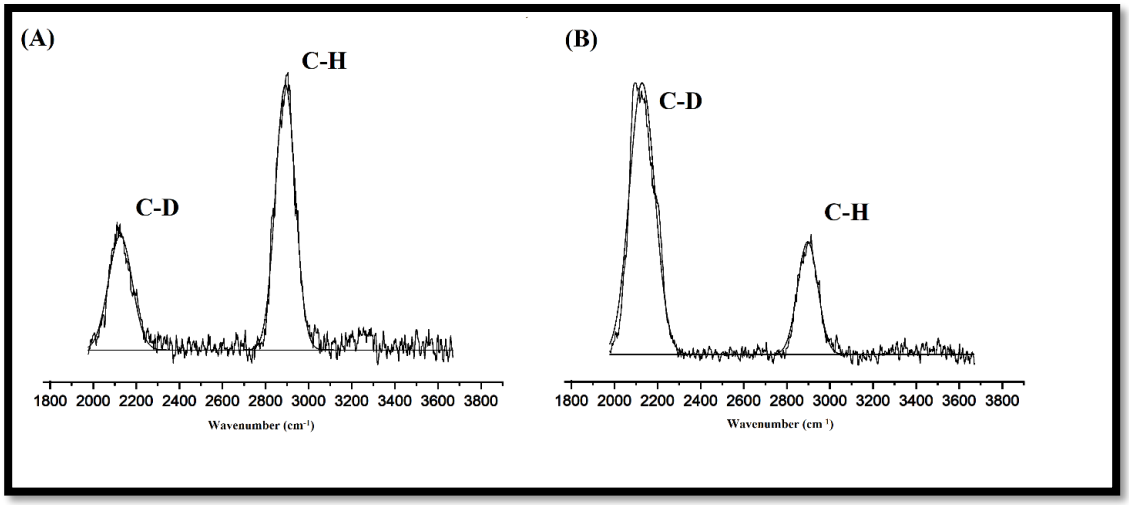

Figure 4: Peak fitting of the Raman spectra of the biomass gown in (A) glucose-D_7 – H_2O (B) glucose-D_7 -D_2O